Mapping the dynamic genetic regulatory architecture of *HLA* genes at single-cell resolution

Joyce B. Kang[1,2,3,4,5], **Amber Z. Shen**[1,2,3,4,5], **Saisriram Gurajala**[1,2,3,4,5], **Aparna Nathan**[1,2,3,4,5], **Laurie Rumker**[1,2,3,4,5], **Vitor R. C. Aguiar**[4,6], **Cristian Valencia**[1,2,3,4,5], **Kaitlyn A. Lagattuta**[1,2,3,4,5], **Fan Zhang**[1,2,3,4,5,7], **Anna Helena Jonsson**[5], **Seyhan Yazar**[8], **Jose Alquicira-Hernandez**[8], **Hamed Khalili**[9], **Ashwin N. Ananthakrishnan**[9], **Karthik Jagadeesh**[10], **Kushal Dey**[10,11,12],

Accelerating Medicines Partnership Program: Rheumatoid Arthritis and Systemic Lupus Erythematosus (AMP RA/SLE) Network[*],

Mark J. Daly[13,14,15,16], **Ramnik J. Xavier**[17,18,19], **Laura T. Donlin**[20,21], **Jennifer H. Anolik**[22], **Joseph E. Powell**[8], **Deepak A. Rao**[5], **Michael B. Brenner**[5], **Maria Gutierrez-Arcelus**[4,6], **Yang Luo**[1,2,3,4,5,23], **Saori Sakaue**[1,2,3,4,5], **Soumya Raychaudhuri**[1,2,3,4,5]

[1]Center for Data Sciences, Brigham and Women's Hospital, Boston, MA, USA

[2]Division of Genetics, Department of Medicine, Brigham and Women's Hospital and Harvard Medical School, Boston, MA, USA.

[3]Department of Biomedical Informatics, Harvard Medical School, Boston, MA, USA.

[4]Program in Medical and Population Genetics, Broad Institute of MIT and Harvard, Cambridge, MA, USA.

[5]Division of Rheumatology, Inflammation, and Immunity, Department of Medicine, Brigham and Women's Hospital and Harvard Medical School, Boston, MA, USA.

[6]Division of Immunology, Boston Children's Hospital, Harvard Medical School, Boston, MA, USA.

[7]Division of Rheumatology and the Center for Health Artificial Intelligence, University of Colorado School of Medicine, Aurora, CO, USA.

[8]Garvan Institute of Medical Research, Sydney, New South Wales, Australia.

[9]Division of Gastroenterology, Massachusetts General Hospital and Harvard Medical School, Boston, MA, USA.

[10]Harvard T. H. Chan School of Public Health, Boston, MA, USA.

[11]Computational and Systems Biology Program, Sloan Kettering Institute, Memorial Sloan Kettering Cancer Center, New York, NY, USA.

[12]Physiology, Biophysics and Systems Biology Program, Weill Cornell Medicine, New York, NY, USA.

[13]Psychiatric and Neurodevelopmental Genetics Unit, Massachusetts General Hospital, Boston, MA, USA.

[14]The Stanley Center for Psychiatric Research, The Broad Institute of MIT and Harvard, Cambridge, MA, USA.

[15]Institute for Molecular Medicine Finland (FIMM), University of Helsinki, Helsinki, Finland.

[16]Analytic and Translational Genetics Unit, Department of Medicine, Massachusetts General Hospital, Boston, MA, USA.

[17]Klarman Cell Observatory, Broad Institute of Harvard and MIT, Cambridge, MA, USA.

[18]Center for Computational and Integrative Biology, Massachusetts General Hospital and Harvard Medical School, Boston, MA, USA.

[19]Department of Molecular Biology, Massachusetts General Hospital and Harvard Medical School, Boston, MA, USA.

[20]Hospital for Special Surgery, New York, NY, USA.

[21]Weill Cornell Medicine, New York, NY, USA.

[22]Department of Medicine, University of Rochester Medical Center, Rochester, NY, USA.

[23]Kennedy Institute of Rheumatology, University of Oxford, Oxford, UK.

Abstract

The human leukocyte antigen (HLA) locus plays a critical role in complex traits spanning autoimmune and infectious diseases, transplantation and cancer. While coding variation in *HLA* genes has been extensively documented, regulatory genetic variation modulating *HLA* expression levels has not been comprehensively investigated. Here we mapped expression quantitative trait loci (eQTLs) for classical *HLA* genes across 1,073 individuals and 1,131,414 single cells from three tissues. To mitigate technical confounding, we developed scHLApers, a pipeline

to accurately quantify single-cell *HLA* expression using personalized reference genomes. We identified cell-type-specific *cis*-eQTLs for every classical *HLA* gene. Modeling eQTLs at single-cell resolution revealed that many eQTL effects are dynamic across cell states even within a cell type. *HLA-DQ* genes exhibit particularly cell-state-dependent effects within myeloid, B and T cells. For example, a T cell *HLA-DQA1* eQTL (rs3104371) is strongest in cytotoxic cells. Dynamic *HLA* regulation may underlie important interindividual variability in immune responses.

The human leukocyte antigen (HLA) genes, located within the major histocompatibility complex (MHC) region on chromosome 6, are central to the immune response. Classical HLA class I and II molecules trigger adaptive immunity by presenting antigens to CD8^{+} and CD4^{+} T cells, respectively. Positive and balancing selection has made the coding sequences of these genes among the most polymorphic in the genome[1]. The *HLA* locus has the greatest number of associations with immune-mediated diseases and typically has larger effect sizes than all other loci combined[1-4]. For example, the *HLA-C*06:02* allele is the major genetic risk factor for psoriasis[5], and *HLA-DRB1* alleles modulate risk for rheumatoid arthritis (RA)[6] and multiple sclerosis[7]. *HLA* genes also play key roles in cancer by presenting neoantigens and in transplantation, where mismatched *HLA* alleles can result in rejection.

The regulatory mechanisms governing *HLA* genes are not yet well understood. Previous studies have focused on coding variation altering HLA protein structure, which may affect antigen binding[6,8,9] or restrict the T cell receptor repertoire[10-12]. However, mounting evidence indicates that noncoding *HLA* regulatory variation can influence disease[13-15]. Higher *HLA-C* expression was found to control HIV infection but increase Crohn's disease risk[13]. Investigators have argued that risk alleles for systemic lupus erythematosus and vitiligo lie within regulatory regions that increase class II expression in myeloid cells[14,15]. Understanding the role of noncoding *HLA* variation in disease requires defining the genetic variation regulating *HLA* gene expression. Previous bulk RNA-sequencing (RNA-seq) studies have identified expression quantitative trait loci (eQTLs) for *HLA* genes in homogeneous cell lines[16,17]. However, *HLA* gene regulation may be context dependent, varying across cell types or finer-grained cell states within a cell type. For example, we previously demonstrated that allele-specific expression of *HLA* class II changes dynamically in activated memory CD4^{+} T cells in vitro[18]. Single-cell RNA-seq (scRNA-seq) may offer a more comprehensive understanding of *HLA* expression and its regulation by assaying cell states in vivo and mapping context-dependent eQTLs[19-21].

Because *HLA* genes are highly polymorphic, standard short-read sequencing pipelines that align reads to a single reference genome are biased when quantifying *HLA* expression[22,23]. Reads can fail to align if an individual's allele is dissimilar from the reference allele, resulting in unmapped reads, or reads can 'multi-map' to multiple *HLA* genes due to sequence similarity between genes[24]. This bias confounds eQTL analysis, making it difficult to distinguish genuine genetic associations with *HLA* expression from inaccurate read alignment. In bulk data, personalized reference genomes accounting for individuals' *HLA* genotypes have been used to overcome this bias[16,17,25,26]. In this Analysis, we developed a personalized pipeline (scHLApers; Fig. 1c) extending this approach to single-cell data. We integrated four datasets (Fig. 1a) to explore how genetic regulation of classical *HLA*

class I (*HLA-A, HLA-B* and *HLA-C*) and class II (*HLA-DPA1, HLA-DPB1, HLA-DQA1, HLA-DQB1* and *HLA-DRB1*) gene expression varies dynamically across diverse immune cell states (Fig. 1d), offering new insights into complex diseases.

Results

Quantifying single-cell *HLA* expression with scHLApers

We developed scHLApers, a pipeline that accurately quantifies single-cell *HLA* expression using a personalized reference (Fig. 1c, Methods and Supplementary Note 1). First, scHLApers uses an individual's unique classical *HLA* alleles (Fig. 1b) to add the personalized genomic sequences for each two-field allele from the Immuno Polymorphism Database-ImMunoGeneTics/HLA (IPD-IMGT/HLA) database[27] to the standard reference genome in place of the original *HLA* gene sequences. scHLApers then uses STARsolo[28] to quantify whole-transcriptome expression in single-cells with multimapping.

Four cohorts with genotype and scRNA-seq data

To study immune cell states from diverse tissues and biological conditions, including some from disease conditions, we used four scRNA-seq datasets with paired genotype data (Fig. 1a, Supplementary Table 1 and Supplementary Fig. 1). After quality control (QC) (Methods and Supplementary Table 2), the combined dataset of 1,073 individuals comprised synovial joint biopsies from an RA cohort[29] (synovium, $n = 69$ individuals), intestinal biopsies from an ulcerative colitis (UC) cohort[30] (intestine, $n = 22$), peripheral blood mononuclear cells (PBMCs) from healthy males cultured in vitro with influenza A virus and control conditions[31] (PBMC-cultured, $n = 73$), and PBMCs from a large Australian cohort[32] (PBMC-blood, $n = 909$).

Imputing *HLA* alleles and MHC variants

Using SNP2HLA with our group's multi-ancestry *HLA* reference panel[24,33,34] (Methods, Fig. 1b and Supplementary Fig. 2), we inferred a common set of 12,050 variants in the MHC with imputation dosage $R^2 > 0.8$ and minor allele frequency (MAF) >1% in each cohort. These included 11,938 single nucleotide polymorphisms (SNPs) and 112 one- and two-field alleles for classical *HLA* genes (Fig. 2a and Supplementary Table 3). We used the two-field alleles to quantify expression with scHLApers (Fig. 1c), and we used both types of variation as input for downstream eQTL analysis (Fig. 1d).

Assessing the performance of scHLApers

We assessed the performance of scHLApers compared to a pipeline without personalization, that is, using the standard GRCh38 reference genome (Methods and Extended Data Fig. 1). We expected estimated *HLA* gene expression to generally increase with scHLApers since it rescues previously unmapped reads. For each individual, we calculated the percentage change in the total unique molecular identifier (UMI) count for each *HLA* gene across all cells after personalization. Personalization indeed generally led to higher estimated expression (Fig. 2b), with concordant trends across cohorts (Extended Data Fig. 1b). We reasoned that if scHLApers aligns reads more appropriately, then personalization should have larger effects for individuals whose alleles diverge more from reference genome alleles.

Encouragingly, for individuals homozygous for the reference allele for a given gene (for example, *HLA-DRB1*15:01*), the scHLApers estimate highly coincided with the standard pipeline's estimate; in contrast, greater dosage of non-reference alleles led to greater changes in estimated expression after personalization (Fig. 2b). To further quantify this, we compared the percentage change in estimated expression per individual to their alleles' sequence dissimilarity to the reference (based on Levenshtein distance, Methods). For all genes except *HLA-B*, individuals with alleles more different from the reference tended to show a greater increase in expression after personalization (Extended Data Fig. 1c). The genes whose expression increased the most per individual were *HLA-DRB1* (mean +29% change, 25th to 75th percentile (+10% to 38% change) in synovium), *HLA-DQA1* (+29% (+3% to 44%)), *HLA-C* (+26% (+5% to 44%)), and *HLA-DQB1* (+7% (+3% to 10%)), consistent with prior findings in bulk RNA-seq[17]. Expression of *HLA-DPB1, HLA-DPA1* and *HLA-A* also increased but to a lesser extent (Supplementary Table 4). Unexpectedly, we observed an overall decrease in *HLA-B* counts across all cohorts (Extended Data Fig. 1b). After detailed investigation, we determined this was not a mishandling of reads by scHLApers, but rather was explained by scHLApers improving the assignments of reads from *HLA-B* to *HLA-C* (Supplementary Note 1). For individuals with both *HLA-C* alleles similar to the reference allele (*HLA-C*07:02*), *HLA-B* was less affected by personalization (Extended Data Fig. 1e). In contrast, for individuals with at least one non-reference-like *HLA-C* allele (that is, different from *HLA-C*07:02*), more reads aligning to *HLA-B* in the standard pipeline aligned better to *HLA-C* in scHLApers, leading to appropriately decreased *HLA-B* counts observed after personalization.

To assess if scHLApers improved the consistency of expression quantification, we leveraged the fact that each PBMC-cultured library was sequenced using two read lengths (289 bp and 84bp). We reasoned that a standard pipeline might lead to inconsistent quantification between the longer and shorter read versions of the dataset due to different types of mapping biases for different read lengths. In contrast, personalization should result in consistent quantification of each *HLA* gene between the two versions. Indeed, personalization increased the correlation between the estimated expression in shorter- and longer-read data for all genes across samples (Fig. 2c; *HLA-B* Spearman $r = 0.97$ scHLApers versus 0.82 standard; *HLA-C* $r = 0.96$ versus 0.86; *HLA-DPB1* $r = 0.97$ versus 0.70). Together, our results demonstrate that aligning reads to a personalized reference improves precision in quantifying single-cell *HLA* expression.

While all four datasets were sequenced using 10x Genomics (10x) 3′ protocols, we also applied scHLApers to a separate dataset of synovium samples with matched 10x 5′ data ($n = 9$ individuals, 26,638 cells)[35]. We found that scHLApers led to a greater increase in *HLA-A* and *HLA-B* counts after personalization in 5′ data compared to 3′ data, due to increased dissimilarity from the reference allele on the 5′ end of the genes compared to the 3′ end (Supplementary Note 1, Supplementary Table 5 and Supplementary Fig. 3).

HLA gene expression across major cell types

After removing low-quality cells (Supplementary Table 2, Supplementary Note 2 and Supplementary Fig. 4a-c), we grouped cells from the four datasets into six major cell types

(Methods and Supplementary Table 6) to investigate cell-type-specific *HLA* expression using scHLApers. These include four immune cell types from all cohorts: 145,090 myeloid cells (monocytes, macrophages and dendritic cells (DCs)), 180,935 B cells (including plasma cells), 805,389 T cells and 125,865 natural killer (NK) cells. It also includes stromal cells from the two solid tissue datasets: 82,651 fibroblasts and 26,300 endothelial cells. We examined *HLA* gene expression patterns across cell types. As expected, we found that all cell types highly express *HLA* class I genes across tissues, consistent with ubiquitous presentation of self-peptides, whereas class II expression varied (Fig. 2d). Specifically, myeloid cells and B cells expressed the highest levels of class II, consistent with their role as professional antigen-presenting cells. Interestingly, all other cell types, such as T cells, also express class II genes, albeit at lower levels. Human T cells have been previously observed to express *HLA* class II upon activation[18,36-38], though its function is not well understood[39-41].

Multi-cohort analysis identifies *HLA* regulatory variants

To identify eQTLs for classical *HLA* genes, we tested the 12,050 MHC-wide variants (Fig. 3a and Supplementary Table 7) for association with the expression of each *HLA* gene in myeloid, B and T cells. We chose these three cell types because they are well represented in all datasets and have known roles in antigen presentation (myeloid and B) or prior evidence for state-dependent *HLA* regulation (T)[18]. For each cell type and individual, we aggregated single-cell expression profiles into a single 'pseudobulk' measurement (Methods and Supplementary Fig. 4d,e). We used linear regression and analyzed all four cohorts together, controlling for covariates and testing 289,200 pairs of variants and *HLA* genes (Methods, Supplementary Fig. 5 and Supplementary Data 1).

We detected an eQTL for every *HLA* gene in every cell type (P values $<4 \times 10^{-9}$; Fig. 3b-e, Supplementary Fig. 6 and Supplementary Table 8). Calculating the effect size of each lead eQTL in each cohort separately, we observed 91.7% (88/96) mean directional concordance across cohorts (Fig. 3d and Supplementary Table 9), suggesting consistent effects across datasets. The B cell results were highly concordant with a previous study on *HLA* eQTLs[17], which used bulk RNA-seq data from lymphoblastoid cell lines and found that all eight variants included in both studies showed consistent directions of effect (Pearson $r = 0.92$, Extended Data Fig. 2a).

Most lead variants (19/24) were individual SNPs within the MHC. For example, rs3104413, the lead variant for *HLA-DQA1* in myeloid cells, is located between *HLA-DRB1* and *HLA-DQA1* ($P = 8.04 \times 10^{-127}$; Fig. 3b,c). This SNP commonly co-occurs with the classical *HLA-DQA1*03:01* allele (87.5% of *DQA1*03:01* haplotypes are in phase with the G allele of rs3104413; Supplementary Table 10). The *HLA-DQA1*03:01* allele is part of the DQ8 haplotype, which is associated with type 1 diabetes and celiac disease[42].

Some lead eQTLs were individual one- or two-field *HLA* alleles. For example, *HLA-B*15* was the lead eQTL for *HLA-B* in all three cell types ($P < 3 \times 10^{-81}$) and associated with lower expression of *HLA-B* (Extended Data Fig. 2b,c). A recent study using a new capture RNA-seq method also found that *HLA-B*15* alleles were among the lowest expressed in bulk PBMCs, consistent with our observations[43]. *HLA-C*07* was the most significant

variant for *HLA-C* in B cells ($P = 2.87 \times 10^{-210}$; Supplementary Fig. 6b and Extended Data Fig. 2b), reflecting reduced expression of *HLA-C*07* alleles relative to other *HLA-C* alleles. This finding could not be explained by read alignment bias (Extended Data Fig. 2c) and is supported by previous work showing that *HLA-C*07* alleles contain a 3′ untranslated region microRNA binding site that reduces *HLA-C* expression[44,45]. Interestingly, the *HLA-C*06:02* and *HLA-C*12:03* alleles, major risk factors for psoriasis[5], were associated with higher *HLA-C* expression in all three cell types ($P < 8 \times 10^{-40}$ and 3×10^{-8}, respectively; Supplementary Data 1). The increased expression of these *HLA-C* alleles may contribute to psoriasis disease risk[46].

scHLApers improves eQTL estimates

We compared the eQTL effect sizes estimated using expression values from scHLApers versus the standard pipeline. For genes whose expression were most affected by personalization, eQTL estimates were meaningfully impacted (Pearson $r = 0.73$ for *HLA-DRB1*, 0.76 for *HLA-DQA1*, 0.76 for *HLA-B*, 0.93 for *HLA-C*; Extended Data Fig. 3a). These improved eQTL estimates probably reflect the reduction of spurious eQTL signals caused by reference bias. For example, using the standard pipeline, the two-field allele *HLA-DRB1*07:01* was significantly associated with *HLA-DRB1* expression in B cells ($\beta = -0.50$, $P = 3.43 \times 10^{-26}$). However, with scHLApers, the effect was corrected away ($\beta = 0.02$, $P = 0.73$) (Extended Data Fig. 3b,c). In contrast, the lead *HLA-DRB1* eQTL for scHLApers (rs9271117) was significant in both pipelines (Extended Data Fig. 3b,c).

HLA eQTLs are cell type dependent

We next explored whether *HLA* eQTLs are cell type dependent, as reported for other genes[32,47]. To test this, we used a mixed-effects model including an interaction term for cell type with genotype (Methods). Almost all (22/24) eQTLs exhibited statistically significant cell-type dependency (interaction $P < 2.08 \times 10^{-3} = 0.05/24$ tests), and several showed dramatic effects (Supplementary Table 11). The strongest example was the lead eQTL for *HLA-DRB1* in B cells (rs9271117, $\beta = 0.7$, $P = 1.08 \times 10^{-128}$), which was ~3-fold weaker in myeloid cells ($\beta = 0.27$, $P = 8.44 \times 10^{-22}$) and altogether absent in T cells ($P = 0.90$) (Fig. 3e). Similarly, eQTLs for *HLA-DPA1* and *HLA-DPB1* (rs2163472 and rs2395305) exhibited much stronger regulatory effects in B cells compared to myeloid and T cells (Supplementary Fig. 8a,b, $\beta = 0.43$ in B versus 0.04 and 0.08 in myeloid and T; $\beta = 0.55$ versus 0.07 and 0.12, respectively). These results highlight the importance of considering cell type when studying the genetic basis of *HLA* expression.

Conditional analysis identifies multiple eQTLs per gene

We used conditional analysis to identify additional regulatory variants beyond the primary eQTL (Supplementary Data 2). For example, after controlling for the effect of rs3104413, a secondary independent variant (rs9272294, linkage disequilibrium (LD) $r^2 = 0.04$ with rs3104413) located ~1.4 kb upstream of *HLA-DQA1* was also associated with *HLA-DQA1* expression in myeloid cells ($P = 3.06 \times 10^{-58}$; Fig. 3c). We repeated this process to identify up to three additional independent eQTLs ($P < 5 \times 10^{-8}$) for each gene in each cell type (Supplementary Fig. 7). *HLA-B*, *HLA-C* and *HLA-DQB1* exhibited the most independent signals (three or more eQTLs per cell type). Most associations (76% = 44/58) were unique

to a gene and cell type ($r^2 < 0.8$ with all other lead variants; Supplementary Fig. 8c), but some were shared. For example, the primary eQTLs for *HLA-DPA1* and *HLA-DPB1* in B cells (rs2163472 and rs2395305, respectively) were tightly linked to each other ($r^2 = 1.0$) and to the secondary signal for *HLA-DPB1* in T cells (rs4435981, $r^2 = 0.99$). Additionally, the primary eQTLs for *HLA-DQA1* in myeloid and T cells (rs3104413 and rs3104371) were linked ($r^2 = 0.86$), and the secondary signals shared the same lead variant (rs9272294).

HLA genes exhibit cell-state-dependent expression

We next investigated whether *HLA* expression varies across cell states. Here, 'cell state' refers to finer-grained transcriptional phenotypes of cells within a major cell type. While there are multiple ways to represent cell state, we used harmonized expression principal components (hPCs) as latent variables capturing the main axes of transcriptional variation among the cells corrected for technical covariates. We integrated the single cells from all four datasets into a unified, continuous, low-dimensional embedding space for each cell type (myeloid, B or T) (Fig. 4a-c). This integration was accomplished by applying PC analysis to the two tissue datasets and removing batch and dataset-specific effects using Harmony[48], then projecting the cells from the two PBMC datasets onto the same hPC axes using Symphony[49] (Methods and Supplementary Fig. 9). The resulting hPC space appropriately captured transcriptional variation as reflected by the cell state annotations from the original studies (Fig. 4d and Supplementary Fig. 13), but does not rely on a specific clustering resolution.

The shared single-cell embedding allowed us to compare *HLA* expression patterns across fine-grained transcriptional states. Both class I and II expression varied widely across cell states within a given cell type (Fig. 4a-c and Supplementary Figs. 10-12). By quantifying the variance explained by cell state for each gene (Methods), we found that cell state generally explained a greater proportion of variance in class II expression (mean 30%, 25th to 75th percentile (17–37%) across all cohorts) compared to class I (mean 19% (8–34%)) (Fig. 4e and Supplementary Table 12). The abundance of certain cell states differed considerably between blood and tissues. For example, tissue macrophages and infiltrating monocytes were absent or at low abundance in PBMCs. However, *HLA* expression patterns were generally similar in cell states shared across tissues, suggesting that cell state rather than tissue context was driving expression. For example, conventional DC1 and DC2 cells expressed the highest levels of class II among myeloid cells in both blood and tissue (Fig. 4a). Among B cells (Fig. 4b), class II expression was lower in plasma cells than in B cells, reflecting the downregulation of class II in the transition to plasma cells[50,51]. Among T cells, proliferating and $CD8^+$ cytotoxic cells expressed the highest levels of class II (Fig. 4c).

Modeling dynamic eQTLs at single-cell resolution

Single-cell-resolution eQTL models[19,20,52,53], which model expression in individual cells, can identify dynamic eQTLs–regulatory effects that change as cells transition across continuous cell states. Dynamic effects can be masked in pseudobulk analysis and may reflect cell-state-specific transcription factors binding to specific regulatory elements.

To investigate whether *HLA* eQTLs are dynamic, we used a single-cell negative binomial mixed-effects (NBME) model (Methods). Briefly, we modeled the UMI count of each gene as a function of genotype and its interaction with cell state, accounting for sample-level covariates (age, sex and ancestry), cell-level fixed effects (library size, percentage mitochondrial UMIs, and expression principal components (PCs)), and random effects for donor and batch (Fig. 5a). The NBME model showed high concordance with the pseudobulk model when testing for eQTL main effect size and significance (Pearson $r = 0.916$ for effect, 0.984 for significance; Extended Data Fig. 4a,b). By simulating single-cell datasets across a range of allele frequencies with different eQTL effect sizes (Methods), we determined that the NBME model has adequate power to detect eQTLs for our application (Extended Data Fig. 4c). We then used the top ten hPCs for each major cell type (Methods) as a continuous multivariate representation of cell state when modeling eQTLs and tested for cell-state interactions ($G \times hPC$) within each dataset using the same cell-state definitions across datasets. We tested the lead eQTLs identified by our pseudobulk analysis, comprising 58 variant-gene pairs with robust genotype main effects and excluding the Intestine dataset due to its small sample size (Methods). We confirmed that the model has well calibrated type I error when testing for cell-state interactions (Extended Data Fig. 4d,e).

We observed that most eQTLs (78% = 45/58) showed statistically significant cell-state dependence (interaction $P < 8.6 \times 10^{-4} = 0.05/58$ tests; Supplementary Table 13). Indeed, every *HLA* gene tested was dynamic in at least one cell type, and *HLA-DQA1, HLA-DQB1, HLA-C* and *HLA-A* were the most state dependent (Supplementary Table 14). Most interaction effects were modest relative to the main genotype effect (Supplementary Table 13). Interestingly, the PBMC-cultured dataset exhibited much less significant cell-state interactions overall (Fig. 5b), despite being similar in size to the synovium dataset. This is possibly due to cell state differences in cultured cells compared to cells collected in vivo.

Comparing dynamic effects across cell states

We next assessed the strength of dynamic regulatory effects in relation to annotated cell states. For each eQTL, we calculated each cell's estimated total eQTL effect size (β_{total}) from the genotype main effect and interaction effects weighted by the cell's position along each hPC (Methods)[19]. This allowed us to compare the eQTL's strength across cell states. For example, in PBMC-blood T cells, the effect of the *HLA-A* eQTL (rs7747253, interaction $P = 4.9 \times 10^{-68}$) was strongest in proliferating cells (mean $\beta_{total} = 0.23$ for proliferating versus 0.10 for other T cells; Fig. 5c), suggesting the variant plays a more substantial role in regulating *HLA-A* expression during T cell proliferation than at rest. This eQTL was also cell state dependent in myeloid cells (Supplementary Fig. 14a-d).

We explored whether cell-state-interacting eQTLs may contribute to interactions with contextual factors that have been tested in bulk-level analyses[47,54-56], including age, sex and interferon response. Our findings indicate that if an eQTL interacts with cell states whose abundance changes with a sample-level factor, the factor can show an interaction in bulk; however, single-cell interaction testing is better powered (Supplementary Note 3, Supplementary Table 15 and Supplementary Fig. 15).

We observed the most significant cell-state interaction effects for *HLA-DQ* genes (Fig. 5b), specifically *HLA-DQA1* in T cells (interaction $P = 2.9 \times 10^{-200}$ in PBMC-blood) and *HLA-DQA1* and *HLA-DQB1* in myeloid cells (interaction $P < 1 \times 10^{-195}$ in both synovium and PBMC-blood). In T cells (Fig. 5d-f), the *HLA-DQA1* eQTL (rs3104371) had the strongest effects in gamma-delta ($\gamma\delta$), cytotoxic CD8$^+$ and cytotoxic CD4$^+$ T cells, a finding that replicated in synovium (Fig. 5f). All three of these cell states exhibit cytotoxic activity. Our results indicate that *HLA-DQA1* expression is under dynamic genetic regulation in T cells, and further studies to clarify its functional role are warranted.

In myeloid cells, PBMC-blood and synovium showed similar patterns of regulation for the *HLA-DQA1* eQTL (rs3104413; Fig. 6a-c). The strongest effects were observed in a subpopulation of monocytes in PBMC-blood and infiltrating monocytes and DC4 cells (which are similar to CD16$^+$ monocytes[57]) in synovium (Fig. 6c), suggesting that the underlying regulatory mechanisms governing the dynamic eQTL are active in both blood and synovium. The estimated β_{total} values were robust to whether the embedding was defined using the tissue datasets or PBMC-blood dataset alone (Pearson *r* across cells, 0.896; Supplementary Fig. 14e-g). In contrast to the T cell *HLA-DQA1* example, the eQTL strength was negatively correlated with the expression of the gene. That is, the expression of *HLA-DQA1* is highest in conventional DC1 and DC2 cells, but the eQTL is weakest in those states (Fig. 6c). *HLA-DQB1* also showed similar patterns of eQTL strength as *HLA-DQA1* in PBMC-blood (*r* across cells, 0.953), suggesting that *HLA-DQ* genes are coordinately regulated.

In B cells, the *HLA-DQA1* and *HLA-DQB1* eQTLs (rs9271375 and rs927346) were also state dependent (interaction $P < 2 \times 10^{-9}$ in synovium and PBMC-blood), with plasma cells and plasmablasts exhibiting the strongest effects (Fig. 6d-f). Interestingly, the overall trend in B cells was similar to myeloid cells (and opposite of T cells) in that cell states with higher *HLA-DQ* expression (pre-activated B cells and conventional DCs, respectively) had weaker eQTL effects. In contrast, states with lower expression (plasma cells and monocytes) had stronger effects. A potential explanation is that cells critical for antigen presentation, such as DCs and pre-activated B cells[58,59], have mechanisms to maintain high *HLA-DQ* expression to ensure proper function, such that genetic effects contribute less to expression differences. Meanwhile, cell states with lower expression may have evolved greater genetic diversity in their antigen presentation capabilities, leading to diversity in immune responses across individuals.

Discussion

This study demonstrates highly variable cell-type and cell-state-specific expression and genetic regulation of *HLA* genes. By integrating four diverse datasets from multiple tissues capturing a broad set of cell states and contexts, we found that classical *HLA* gene expression is under *cis*-regulation. Class II genes show particularly variable strengths of genetic regulation depending on cellular context. At the cell-type level, B cells display much stronger regulatory effects for *HLA-DRB1, HLA-DPA1* and *HLA-DPB1* than myeloid and T cells (Fig. 3e and Supplementary Fig. 8a,b). Single-cell resolution eQTL modeling revealed that many eQTLs are cell state dependent, especially for *HLA-DQ* genes (Figs. 5

and 6). We previously showed that *HLA-DQ* exhibits state-dependent regulation in CD4^{+} T cells ex vivo[18]. Here, we demonstrated that *HLA-DQ* is dynamically regulated in multiple cell types across tissues in vivo.

Variation in the HLA is hypothesized to have evolved to confer selective advantages in immune response to pathogens[60], maternal–fetal tolerance[61] and susceptibility to autoimmune diseases[62], depending on environmental contexts. Coding variation in *HLA* genes affects the quality of presented antigens by determining which peptide sequences are presented, and population diversity enables collective responsiveness to diverse pathogens. Concurrently, *HLA* regulatory variation may affect the quantity of antigen presentation, leading to different thresholds of immune responsiveness. It has been shown that the expression levels of *HLA-C* alleles can affect immunogenicity in unrelated donor hematopoietic cell transplantation[63], and *HLA* downregulation in tumors may affect response to immune checkpoint inhibitors[64,65]. The presence of multiple independent regulatory effects at each *HLA* gene and cell-type and cell-state-specific effects suggests that regulatory variation may have been selected to ensure diverse immune responses within a population.

There are several limitations of this study. First, our reference-based HLA imputation may have missed ultra-rare alleles. Long-read sequencing or sequence-based typing with polymerase chain reaction could eventually improve the detection of all possible noncoding *HLA* variants[66,67]. Second, we were not able to fine-map the eQTLs to precise causal variants because of the high degree of linkage disequilibrium (LD) in the MHC region. Functional work evaluating candidate causal variation may ultimately define causal variation. Finally, we did not perform colocalization with genome-wide association study associations for several reasons. Standard tools (for example, coloc[68]) that assume a single causal variant are not appropriate within the *HLA* locus because genome-wide association study signal may jointly arise from both coding and regulatory variation, rather than acting exclusively through gene expression. Moreover, although colocalization can be paired with conditional analyses or fine-mapping approaches[69] to test multiple independent effects in a region, the extensive LD poses a challenge. Colocalization analyses within the *HLA* have not been systematically evaluated for accuracy and replication and warrant future investigation.

Future data generation efforts that increase the size and ancestral diversity of genotyped single-cell cohorts will continue to improve our understanding of state-dependent and population-specific regulatory effects and aid in fine-mapping efforts[70].

Methods

Quantifying single-cell *HLA* expression with scHLApers

We developed the scHLApers (single-cell *HLA* expression using a personalized reference) pipeline to accurately quantify classical *HLA* expression in scRNA-seq data. As input, the pipeline takes in scRNA-seq read-level data (FASTQ or BAM) and *HLA* allele calls. If sequence-based typing is unavailable, *HLA* alleles can be imputed using genotyping data (see 'HLA imputation' section). A personalized reference is created for each individual by

adding personalized *HLA* allele sequences as extra contigs to the reference and masking the original reference *HLA* gene sequences. The output is a whole-transcriptome counts matrix with improved *HLA* expression estimates. The code and tutorials to run scHLApers are available at ref. 71 (v1.0 used for this study).

Preparing the *HLA* allelic sequence database.—scHLApers requires a database of genomic *HLA* allele sequences. To prepare this, we downloaded the IPD-IMGT/HLA database[72] (v3.47.0). The database contains sequence alignment files for full-length genomic sequences (that is, four-field resolution, ending in 'gen.txt') and nucleotide coding sequences (that is, two- and three-field resolution, ending in 'nuc.txt'). We filled in any incomplete genomic sequences with bases from the most similar complete allele using the hla_compile_index function from the 'hlaseqlib' R package (v0.0.3)[73]. Coding allele sequences with no corresponding genomic sequence were substituted with the genomic sequence of the most similar allele with a genomic sequence based on the Hamming distance of coding sequences. For *HLA-A*, *HLA-DQA1*, *HLA-DQB1*, *HLA-DPA1* and *HLA-DPB1*, we padded the 5′ and 3′ ends of the allelic sequences from IPD-IMGT/HLA with extra bases from the GRCh38 reference to ensure that they did not have any missing sequence content compared to the reference sequences. The reference gene boundaries were defined by the Gencode v38 annotation file.

Creating personalized reference genome and annotation files.—scHLApers creates a personalized reference genome (FASTA) and annotation file (GTF) for each individual. Based on the *HLA* allele calls, scHLApers creates a FASTA file for each individual with their genomic allelic sequences from the allelic sequence database. Each allele is included as a separate contig, with the allele name as the identifier. If multiple four-field versions exist for a given two-field allele, the corresponding XX:XX:01:01 allele sequence is chosen. The original reference classical *HLA* gene sequences are masked with 'NNN…' to prevent reads from aligning to them. The personalized allelic sequences are then concatenated with the masked GRCh38 reference genome to produce the personalized reference.

In the personalized annotation file (GTF), all entries corresponding to the classical *HLA* genes are removed from the original Gencode v38 annotation file. New entries are added for each personalized allele with the 'seqname' column labeled as the allele name (matching the identifier in the personalized reference FASTA file), the 'feature name' as 'exon' to enable read alignments to the entire sequence, the 'start' and 'end' positions as '1' and the length of the sequence, respectively, and the strand as '+' since all sequences in the database are defined as the forward strand. The 'attribute' column is labeled with 'transcript_id' as the allele name (for example, IMGT_A*01:01:01:01) and 'gene_id' and 'gene_name' as the gene name (for example, IMGT_A), allowing alignments to either allele of the gene to contribute to its total UMI count.

Quantifying single-cell expression.—Using the personalized genome and annotations, scHLApers performs single-cell read alignment and expression quantification using STARsolo[28] (v2.7.10a). STARsolo performs barcode correction, UMI collapsing and optimal distribution of multimapping reads (that is, reads mapping to either overlapping

genes or multiple paralogous genes at separate loci), which are typically discarded in standard pipelines. We chose STARsolo over pseudoalignment-to-transcriptome methods because it can identify splice junctions de novo, which is useful because the transcript isoform usage for each *HLA* allele is not readily available. The personalized genome index is generated using STARsolo –runMode genomeGenerate, and read alignment is performed with –runMode alignReads. The user specifies the appropriate UMI length (–soloUMIlen), cell barcode whitelist file (–soloCBwhitelist), and assay type (–soloType CB_UMI_Simple for droplet-based data). Additionally, scHLApers counts all reads overlapping gene's introns and exons (–soloFeatures GeneFull_Ex50pAS) and optimally distributes multimapping reads using an expectation-maximization algorithm (–soloMultiMappers EM). The parameters –soloCBmatchWLtype 1MM_Nbase_pseudocounts, –soloUMIfiltering MultiGeneUMI_CR and –soloUMIdedup 1MM_CR are used to match CellRanger results. Users can output a coordinate-sorted BAM file to view individual read alignments (–outSAMtype BAM SortedByCoordinate and –outSAMunmapped Within).

Cohorts with paired single-cell transcriptomics and genotype data

We obtained data from four existing studies with scRNA-seq and genotype data from the same individuals (Supplementary Table 1). These include (1) synovial biopsies from patients with RA and from osteoarthritis controls (synovium, $n = 69$ individuals after sample QC)[29], (2) intestinal biopsies from patients with UC and from healthy controls (intestine, $n = 22$)[30], (3) PBMCs from healthy males that were treated in vitro with both influenza A virus and mock conditions (PBMC-cultured, $n = 73$)[31], and (4) PBMCs collected from a large population cohort (PBMC-blood, $n = 909$)[32]. For details regarding the collection of these cohorts and determination of the number of samples per cohort included in this study, see Supplementary Note 4.

QC of genotyping data

All cohorts were genotyped using genotyping arrays, except for PBMC-cultured, which used low-pass whole-genome sequencing (WGS) (Supplementary Table 1). We processed the genotyping data and performed QC using PLINK v1.90, as described in Supplementary Note 4 following the tutorial at ref. 74 (ref. 24). Genome-wide variants were used to calculate PCs to control for genetic ancestry in eQTL analysis, and variants in the extended MHC (defined here as chr 6: 28000000–34000000) were used for HLA imputation.

HLA imputation

HLA imputation with SNP2HLA.—We used SNP2HLA[75] to perform HLA imputation using version 2 of our group's multi-ethnic reference panel described in Sakaue et al.[24,33,34]. We performed imputation on the full genotyping datasets (that is, not limited to samples with paired scRNA-seq), then subset the imputed VCF file to the samples with scRNA-seq. Two types of genetic variation were imputed: SNPs within the MHC ($n = 14,691$) and classical *HLA* alleles at one- and two-field resolution for *HLA-A, HLA-B, HLA-C, HLA-DPA1, HLA-DPB1, HLA-DQA1, HLA-DQB1* and *HLA-DRB1* ($n = 570$). In SNP2HLA

output, reference (REF) and alternative (ALT) values for classical alleles are set to 'A' and 'T' denoting absence and presence of the allele, respectively.

The two-field *HLA* alleles were used in scHLApers to make personalized references. SNP2HLA outputs an individual's imputed dosage (0–2) and inferred genotype (GT: 0|0, 0|1, 1|0 or 1|1) for every *HLA* allele in the reference panel. Note that, for a subset of individuals, we could not confidently call two-field alleles for one or more *HLA* genes, and the dosage was split across multiple alleles (<0.5 for any given allele). We excluded these individuals (9 synovium, 3 intestine, 15 PBMC-cultured and 60 PBMC-blood individuals, representing <8% of total samples) to avoid introducing a technical batch effect. All downstream analyses included 1,073 individuals for whom we could confidently impute phased alleles for every *HLA* gene (GT: 0|1 and 1|0 for two alleles or GT: 1|1 for one allele).

QC of imputed MHC variants.—We performed QC on the imputed MHC-wide variants using custom R scripts and the 'vcfR' (v1.12.0) package. Because the HLA reference uses hg19 coordinates, we first lifted over the imputed variants to GRCh38 using CrossMap (v0.6.1) and chain file[76]. Then, we subset to the relevant samples and calculated the MAF within the subset. We retained variants with imputation dosage R^2 (DR2, the estimated squared correlation between the estimated allele dose and the true allele dose) >0.8 and MAF >0.01 in each cohort. For the intestine cohort, which was genotyped on two different arrays, we first filtered by DR2 within each array then merged them by the intersecting variants before filtering by MAF >0.01 across the merged cohort. We took the intersection of variants across all four cohorts passing our QC thresholds to arrive at a final set of 12,050 variants for eQTL testing (Supplementary Fig. 2): 112 one- and two-field *HLA* alleles and 11,938 intergenic variants.

Assessing the performance of scHLApers

Applying scHLApers to all four cohorts.—We applied scHLApers to quantify single-cell expression for all four datasets. As a comparison, we also ran a standard pipeline that used STARsolo with the same parameters as scHLApers but with the original GRCh38 reference (with no personalization) and discarding multimapping reads. For both versions, we generated BAM files containing unmapped reads (samtools view -b -f 4) and reads aligning to the MHC and personalized contigs using samtools (v1.4.1). We removed empty droplets and low-quality cells by filtering the count matrices by cell barcodes (see 'Processing single-cell expression data' section).

For the read length concordance analysis, the PBMC-cultured dataset contained reads of two different lengths (84 and 289 bp). We generated long- and short-read versions of the dataset by creating separate BAM files by sequence length and running scHLApers on longer and shorter reads separately. To visually inspect read alignments and coverage across the personalized allelic contigs in scHLApers, we used Integrative Genomics Viewer (IGV v2.11.2).

Comparing percent change to dissimilarity from the reference alleles.

We assessed how expression estimates (summed UMI counts across all cells for a sample) changed from a standard pipeline (sp_exp) to the scHLApers pipeline (pers_exp) (equation (1)) with respect to the dissimilarity between the reference allele and personalized alleles.

$$\% \, \text{change} = \frac{\text{pers\_exp} - \text{sp\_exp}}{\text{sp\_exp}}$$

(1)

Dissimilarity was defined as the Levenshtein distance between the genomic GRCh38 allele and personalized allele sequences, calculated using the stringdist function in the 'stringdist' (v0.9.8) R package. Since all datasets used 10x 3′ assays, the read coverage was predominantly at the 3′ end of the gene (Supplementary Fig. 3). Hence, distances were calculated at the 3′ end using sequence segments of 500 bp (*HLA-A, HLA-B, HLA-C* and *HLA-DRB1*), 1,000 bp (*HLA-DQA1* and *HLA-DPA1*), 1,500 bp (*HLA-DQB1*) or 2,500 bp (*HLA-DPB1*), encompassing the region where reads accumulated. For individuals heterozygous for a gene, we took the mean of the two distances. The GRCh38 reference allele sequences are listed in Darby et al.[77] (*A*03:01, B*07:02, C*07:02, DQA1*01:02, DQB1*06:02, DRB1*15:01, DPA1*01:03* and *DPB1*04:01*). We confirmed these by performing a multiple sequence alignment between the IPD-IMGT/HLA allelic sequences and the reference sequence using the msaClustalW function from the 'msa' (v1.22.0) R package.

Application of scHLApers to 5′-based data.—We applied scHLApers to a separate dataset from a subset of synovium individuals with matching 10x 5′ data (*n* = 9 individuals, 26,638 cells)[35]. To compare the dissimilarity of *HLA* class I alleles to the reference alleles at the 5′ end (500-bp region), we calculated Levenshtein distance at the 5′ end of the multiple sequence alignment, as described for 3′ data above.

Investigating read mapping between *HLA-B* and *HLA-C*.—To quantify the rescuing of unmapped reads and identify reads 'jumping' between different genes, we tracked where reads aligned in scHLApers versus the standard pipeline. We analyzed the BAM files output from both pipelines using a custom R script and the scanbam function in 'Rsamtools' (v2.6.0). A given read can align to the classical *HLA* genes (that is, personalized contigs for scHLApers or gene regions defined by Gencode v38 for the standard pipeline), another location in the MHC outside of classical *HLA* genes, another location outside of the MHC, or be unmapped. We used the multiple sequence alignment for *HLA-C* to generate a phylogenetic tree of *HLA-C* allele sequences using the 'Neighbor Joining' option in Jalview (v2.11.0). By grouping the *HLA-C* alleles by similarity to the reference allele (*C*07:02*) based on the tree, we could observe the relationship between the dosage of 'reference-like' *HLA-C* alleles and the change in *HLA-B* counts.

Processing single-cell expression data

QC of single-cell data.—For synovium, intestine and PBMC-cultured datasets, we subset the count matrix output from scHLApers to the cells passing QC in the original studies (that is, barcodes present in published cell metadata). For the PBMC-blood dataset, we started from the original cells but performed additional filtering steps to remove suspected doublets (Supplementary Note 2). Then, we performed uniform cell-level QC procedures on all cohorts, removing cells with <500 genes and >20% mitochondrial counts.

Defining major cell types and merged cell annotations.—We defined a common set of six major cell types across the four datasets–myeloid (monocytes, macrophages and DCs), B (including plasma), T, NK, fibroblast and endothelial–by aggregating fine-grained cell annotations. For synovium, intestine and PBMC-cultured, these fine-grained annotations came from the originally published cell annotations. For PBMC-blood, we used the Seurat Azimuth PBMC CITE-seq reference[78] to transfer labels to the cells following the more stringent doublet removal (Supplementary Note 2). We removed cells from the following annotations that did not fall under our major cell type categories of interest: 'Mu-0: Mural' and 'T-21: Innate-like' cells in synovium; 'Glia', 'CD69$^-$ Mast', 'CD69$^+$ Mast' and 'Pericytes' for intestine; 'NKT' and 'neutrophils' for intestine; and 'HSPC', 'Platelet', 'Doublet', 'Eryth' and 'MAIT' for PBMC-blood. The final cell numbers can be found in Supplementary Table 2. We generated cell-type-specific count matrices for downstream analyses, removing cells from individuals with fewer than five cells of the cell type. To obtain a version of finer-grained cell annotations to aid in the interpretation of cell embeddings, we manually merged the fine-grained cell annotations for myeloid, B and T cells in synovium and PBMC-blood datasets to a shared set of common cell state annotations (for example, PBMC-blood 'CD4 CTL' and 'CD4 TEM' and synovium 'T-12: CD4$^+$ GNLY$^+$' were merged into 'CD4$^+$ Cytotoxic'; Supplementary Table 6).

Pseudobulk eQTL analysis

Generation of pseudobulk profiles.—For each cell type (myeloid, B and T), we generated 'pseudobulk' versions for each dataset. First, we performed library size normalization using log(CP10k + 1) within each cell, then aggregated all cells per sample by taking the mean normalized expression of each gene to obtain a samples-by-genes matrix[79]. We excluded individuals with fewer than five cells of the cell type. We performed rank-based inverse normal transformation for each gene, including genes with nonzero expression in greater than half of the samples.

Multi-cohort eQTL model.—To control for genetic ancestry, we used PLINK (v1.90) to calculate genotype PCs (gPCs) using 66,827 shared genome-wide variants across all four datasets. For PC analysis, we included all individuals from the full array cohorts passing QC (including those without paired scRNA-seq data, Supplementary Fig. 1f). To infer hidden determinants of gene expression variation, we ran probabilistic estimation of expression residuals (PEER)[80] on each pseudobulk expression matrix for each dataset and cell type separately, using the 'peer' R package (v1.0). We used different numbers of PEER factors (K) for each dataset to account for the varying number of individuals in each cohort ($K = 7$ for synovium, 2 for intestine, 7 for PBMC-cultured and 20 for PBMC-blood; Supplementary

Fig. 5a). We generated covariate-corrected expression residuals, accounting for sex, age, ancestry (five gPCs), 10x chemistry (for intestine) and PEER factors.

To identify eQTLs for each classical *HLA* gene, we incorporated all four datasets into a single model ('multi-cohort model') to boost power. We combined the expression residuals from all datasets together for each cell type (Supplementary Fig. 5b). For PBMC-cultured, which included both influenza-stimulated and noninfected cells for each sample, we included only the noninfected cells in the analysis. We tested each of the 12,050 MHC-wide variants for association with residualized expression (E_{resid}) using linear regression (equation (2)), controlling for the dataset to account for systematic differences across cohorts. This provided a pooled estimate for each eQTL effect across datasets. For lead eQTLs in the multi-cohort model, we also ran the model in each dataset separately (without the dataset term) to compare the concordance across datasets. We also ran the same model using the *HLA* expression estimates from the standard pipeline to compare to the scEIlApers results.

$$E_{\text{resid}} = \beta_{\text{G}} X_{\text{G}} + \beta_{\text{dataset}} X_{\text{dataset}} + \varepsilon$$

(2)

Comparison to Aguiar et al. bulk eQTL study.—We compared the lead eQTL effects identified in this study to a bulk RNA-seq study by Aguiar et al.[17] on *HLA* eQTLs in lymphoblastoid cell lines (LCLs). We obtained eQTL summary statistics from the original authors and limited the comparison to B cells in this study as they are most biologically similar to LCLs. Because some variants tested in this study were not tested in Aguiar et al., we restricted the comparison to the lead variants among those tested in both.

Grouping classical *HLA* alleles by lead eQTL variants.—To determine how classical one- and two-field *HLA* alleles track with lead eQTL variants, we compared the co-occurrence between eQTL variants and *HLA* alleles for the associated gene. To calculate co-occurrence ($\text{Occ}_{\text{allele,eQTL}}$, ranging from 0 to 1), we used the multi-ethnic HLA reference panel dataset from HLA imputation[24]. Because the reference dataset is phased, we could calculate the proportion of reference haplotypes ($n = 20{,}349$ samples $\times$ 2 chromosomes $= 40{,}698$ haplotypes) containing the ALT allele of each lead eQTL using a custom R script (equation (3)).

$$\text{Occ}_{\text{allele,eQTL}} = \frac{\#\text{haplotypes with HLA allele and ALT version of eQTL}}{\text{Total}\,\#\,\text{haplotypes with HLA allele}}$$

(3)

Cell-type interaction analysis.—To determine whether lead eQTLs are cell type dependent, we modeled the residualized expression from all three cell types together using a linear mixed-effects model, adding a fixed effect for cell type (myeloid, B or T), an interaction term between variant and cell type (G × cell_type), and a random effect for donor to account for the non-independent sampling of cell types from the same donor (equation

(4)). To ascertain the significance of the cell type dependency, we compared the full model to a null model without the interaction term using a likelihood ratio test (LRT) (lrtest function from 'lmtest' v0.9-39R package).

$$E_{resid} = \beta_G X_G + \beta_{dataset} X_{dataset} + \beta_{cell\_type} X_{cell\_type}$$
$$+ \beta_{G \times cell\_type} X_{G \times cell\_type} + (\phi_{donor} \mid donor) + \varepsilon$$

(4)

Conditional analysis.—To identify additional eQTLs independent from the lead eQTL, we performed up to three additional rounds of conditional analysis for each gene and cell type using the multi-cohort model, conditioning on the lead eQTL(s) from the previous round(s). We terminated early if the lead eQTL did not reach a significance of $P < 5 \times 10^{-8}$. We used PLINK (v1.90) (–ld) to calculate LD r^2 values between every pair of lead eQTLs across cell types and rounds of conditional analysis using the multi-ethnic HLA reference panel.

Visualizations.—To generate boxplots of pseudobulk eQTL effects, we used the expression residuals and regressed out the effect of dataset (not already corrected during PEER). For the Manhattan plots, because each gene has multiple potential transcription start sites (TSS) depending on the transcript, we selected the transcript with the midpoint chromosomal start position across transcripts. LD r^2 values for the locus zoom plot were calculated using PLINK (v.1.90) and the multi-ethnic HLA reference panel. For generating figures, we used R packages 'ggrastr' (v1.0.1), 'ggrepel' (v0.9.1), 'patchwork' (v1.1.1) and ggplot2' (v3.3.5).

Creating a single-cell atlas of *HLA* expression

Mapping cells into a shared embedding.—To create low-dimensional cell state embeddings of single cells across datasets, we first integrated the two tissue datasets (synovium and intestine). For each cell type (myeloid, B and T), we concatenated the counts matrices from both datasets and filtered to the union of the top 1,500 variable genes per dataset calculated using the variance stabilizing transform (vst) method, excluding cell cycle genes (Seurat v4.1.0s.genes and g2m.genes), mitochondrial (MT-) and ribosomal (RPL-, RPS-) genes. We scaled the variable genes across all cells using R package 'singlecellmethods' (v0.1.0), calculated the top ten PCs (using the 'irlba' v2.3.5 R package), then removed sample and dataset-specific effects using Harmony[48] (v0.1.0) (parameters: $\theta_{sample} = 0.5, \theta_{dataset} = 1$, nclust 50 and sigma 0.2), resulting in a ten-dimensional 'Harmonized PC' (hPC) embedding. We visualized the embedding in 2D using uniform manifold approximation and projection (UMAP), calculated with the umap function in the 'uwot' (v0.1.11) R package, with n_neighbors = 30 and min_dist = 0.2. We then projected the two PBMC datasets into the same tissue-defined embedding using Symphony[49] (v0.1.0) to align analogous cell states across tissues. For PBMC-cultured, we included cells from both influenza-stimulated and noninfected samples. Symphony mapping was performed one query dataset at a time, correcting for 'sample' effects in the query.

As an alternative approach, we also explored de novo integration of all four datasets together. We used the top 1,500 variable genes per dataset (top 1,000 for T cells) and Harmony integration with $\theta_{\text{dataset}} = 0.5$, $\theta_{\text{batch}} = 0.5$ and $\theta_{\text{sample}} = 0.5$ (batch defined as the sample for Synovium, 10x chemistry for intestine, and experimental batch for PBMC datasets). However, the tissue-defined embeddings produced a cleaner visual separation of cell states, particularly for myeloid cells (Supplementary Fig. 9) and were therefore used for downstream analysis.

Quantifying proportion of expression variance explained by cell state.—To estimate the percent of variance in *HLA* expression explained by cell state, we fit an NBME model of the UMI count of each *HLA* gene across cells in each cell type. We included donor-level fixed effects for age, sex and ancestry (five gPCs), cell-level fixed effects for scaled log(total UMI count), scaled percent mitochondrial UMIs, and cell state (ten hPCs), and random effects for donor (and experimental batch for PBMC datasets). The NBME models (including all other versions described in subsequent sections) were fit using the glmer.nb function from the 'lme4' (v1.1-28) R package with options nAGQ = 0 and 'nloptwrap' optimizer. We used the r.squaredGLMM function from the 'MuMIn' (v.1.43.17) R package[81] to estimate the marginal R^2 using the 'delta' method for the full model (equation (5)) as well as a model without cell state terms. The difference between the R^2 values between the two models was used to estimate the proportion of variance explained by cell state.

$$\log(E) = \beta_0 + \beta_{\text{age}} X_{\text{age}} + \beta_{\text{sex}} X_{\text{sex}} + \sum_{k=1}^{5} \beta_{\text{gPC}_k} X_{\text{gPC}_k}$$
$$+ \beta_{\text{nUMI}} \log(X_{\text{nUMI}}) + \beta_{\text{MT}} X_{\text{MT}} + \sum_{k=1}^{10} \beta_{\text{hPC}_k} X_{\text{hPC}_k}$$
$$+ (\phi_{\text{donor}} \mid d) + (\delta_{\text{batch}} \mid b)$$

$$(5)$$

Defining a cell embedding using PBMC-blood alone.—We also defined an alternative cell state embedding for each cell type using cells from PBMC-blood alone. To do this, we used the same dimensionality reduction pipeline described above for the tissue-defined embedding, except we used the top 2,000 variable genes across PBMC-blood for each cell type and corrected for experimental batch with Harmony ($\theta_{\text{batch}} = 2$).

Single-cell eQTL analysis

We used a single-cell NBME eQTL model to test *HLA* eQTLs for cell-state dependency. The model is adapted from the Poisson mixed-effects (PME) model recently described by our group[19]. We used NBME in this study because we found that the LRT *P* values from the PME model exhibited inflation when testing for cell-state interactions (Extended Data Fig. 4d; see 'Evaluating model calibration for testing cell-state interaction' section), probably because *HLA* genes exhibit greater overdispersion than other genes, whereas NBME was well calibrated. We first used an NBME model without cell state to define the set of variant-gene pairs with robust genotype main effects within each dataset. We then used an

NBME model with cell state to test for dynamic effects. We excluded the Intestine dataset due to small sample size ($n = 22$).

Testing for genotype effect using NBME model without cell state.—Using the lead eQTL variants identified in the pseudobulk multi-cohort model above (8 genes × 3 cell types = 24 variants), we tested each eQTL using a single-cell NBME model (equation (6)) to assess the genotype effect. We modeled the per-cell UMI count of each *HLA* gene in each major cell type and dataset separately (24 variants × 3 datasets = 72 variant-gene pairs to test). We included the same donor and cell-level fixed and random effects as in equation (5), except without cell state terms (hPCs) and adding additional terms for donor genotype (G) and five expression PCs (ePCs), which are calculated on each dataset separately to account for technical effects (akin to PEER factors in pseudobulk). We determined the significance of the genotype effect by comparing to a null model without genotype using an LRT with 1 degree of freedom.

$$
\begin{aligned}
\log(E) = {} & \beta_0 + \beta_G X_G + \beta_{age} X_{age} + \beta_{sex} X_{sex} + \sum_{k=1}^{5} \beta_{gPC_k} X_{gPC_k} \\
& + \beta_{nUMI} \log(X_{nUMI}) + \beta_{MT} X_{MT} + \sum_{j=1}^{5} \beta_{ePC_j} X_{ePC_j} \\
& + (\phi_{donor} \mid d) + (\delta_{batch} \mid b)
\end{aligned}
$$

(6)

We compared the genotype main effect size and significance from the NBME model (equation (6)) to the pseudobulk eQTL model using the PBMC-blood dataset. Significance was represented by LRT *P* values in the NBME model and Wald *P* values in the pseudobulk linear model (run on PBMC-blood separately).

To define variants with robust main effects to test for cell-state interaction, we included only variant-gene pairs within a cell type and dataset with a significant genotype main effect (LRT *P* value <0.05), resulting in a total of 58 variant-gene pairs.

Power analysis for NBME model.—We estimated the power to detect a spectrum of effect sizes across a range of allele frequencies using our NBME model (methods detailed in Supplementary Note 4).

Testing for cell-state interaction using NBME model.—To test the 58 variant-gene pairs for dynamic regulatory effects, we modeled the eQTLs at single-cell resolution using an NBME model (equation (7)). While the model can use any cell state variable (for example, clusters and pseudotime trajectory), we reasoned that hPCs would provide a principled and unbiased way to define continuous cell states. We include the same donor and cell-level fixed and random effects as in equation (6), with the addition of cell state (hPC1-10 from the tissue-defined Symphony embeddings) and genotype interaction with cell state (G × hPC1 + … + G × hPC10). To assess whether the eQTL is cell state dependent, we compared the full model (equation (7)) to a null model without interaction terms using an LRT with 10 degrees of freedom.

$$\log(E) = \beta_0 + \beta_G X_G + \beta_{\mathrm{age}} X_{\mathrm{age}} + \beta_{\mathrm{sex}} X_{\mathrm{sex}} + \sum_{k=1}^{5} \beta_{\mathrm{gPC}_k} X_{\mathrm{gPC}_k}$$

$$+ \beta_{\mathrm{nUMI}} \log(X_{\mathrm{nUMI}}) + \beta_{\mathrm{MT}} X_{\mathrm{MT}} + \sum_{j=1}^{5} \beta_{\mathrm{ePC}_j} X_{\mathrm{ePC}_j}$$

$$+ \sum_{k=1}^{10} \beta_{\mathrm{hPC}_k} X_{\mathrm{hPC}_k} + \sum_{k=1}^{10} \beta_{G \times \mathrm{hPC}_k} X_G \times X_{\mathrm{hPC}_k}$$

$$+ (\phi_{\mathrm{donor}} \mid d) + (\delta_{\mathrm{batch}} \mid b)$$

(7)

Evaluating model calibration for testing cell-state interaction.—We analyzed the calibration of the NBME model when testing for interaction between genotype and cell state. Using the PBMC-blood cells and embedding defined in PBMC-blood alone, we permuted cell state (ten hPCs as a block) across all cells, then ran the NBME model for each variant-gene pair (equation (7)) and assessed its significance using LRT, which should yield uniform P values if the model is well calibrated. We repeated this process for 1,000 permutations and compared the results to the equivalent analysis performed with a PME model (glmer function from 'lme4' R package with family = 'poisson').

Comparing eQTL strength across cell states.—For a given eQTL, we combined the genotype main effect (β_G) with the interaction effects of each hPC (estimated in equation (7)), weighted by each cell's position along each hPC (for example, $\beta_{G \times \mathrm{hPC1}} \times \mathrm{hPC1}$) to score each cell on the basis of its estimated total eQTL effect size (equation (8)). This allowed us to compare the strength of the eQTL across cell states by plotting the estimated β_{total} of each cell in UMAP coordinates and comparing the mean β_{total} across cell state annotations.

$$\beta_{\mathrm{total}} = \beta_G + \sum_{k=1}^{10} \beta_{G \times \mathrm{hPC}_k} \mathrm{hPC}_k$$

(8)

By binning cells by five quantiles of estimated β_{total}, we calculated the main genotype effect in each quantile separately (β_{NBME}) using equation (6), determining significance by LRT comparing to a null model without the genotype term. For the T cell *HLA-A* dynamic eQTL, the dynamic effect was very specific to proliferating cells. Hence, for visualization, we did not bin the cells by five quantiles based on hPCs because proliferating cells were rare ($n = $ 739 cells) and instead calculated the main genotype effect in proliferating cells and CD8+ Cytotoxic cells ($n = 96,516$) for comparison.

To compare the β_{total}, estimates derived from the tissue-defined embedding to those from the embedding defined using PBMC-blood alone for the myeloid *HLA-DQA1* eQTL (rs3104413), we ran the same NBME cell-state interaction model (equation (7)) except using ten hPCs defined in PBMC-blood (see 'Defining a cell embedding using PBMC-blood alone' section). We calculated the Pearson correlation between the β_{total} estimates produced

by the two embeddings. We also tested for eQTL interactions with contextual factors (age, sex and interferon response) as described in Supplementary Note 4.

Extended Data
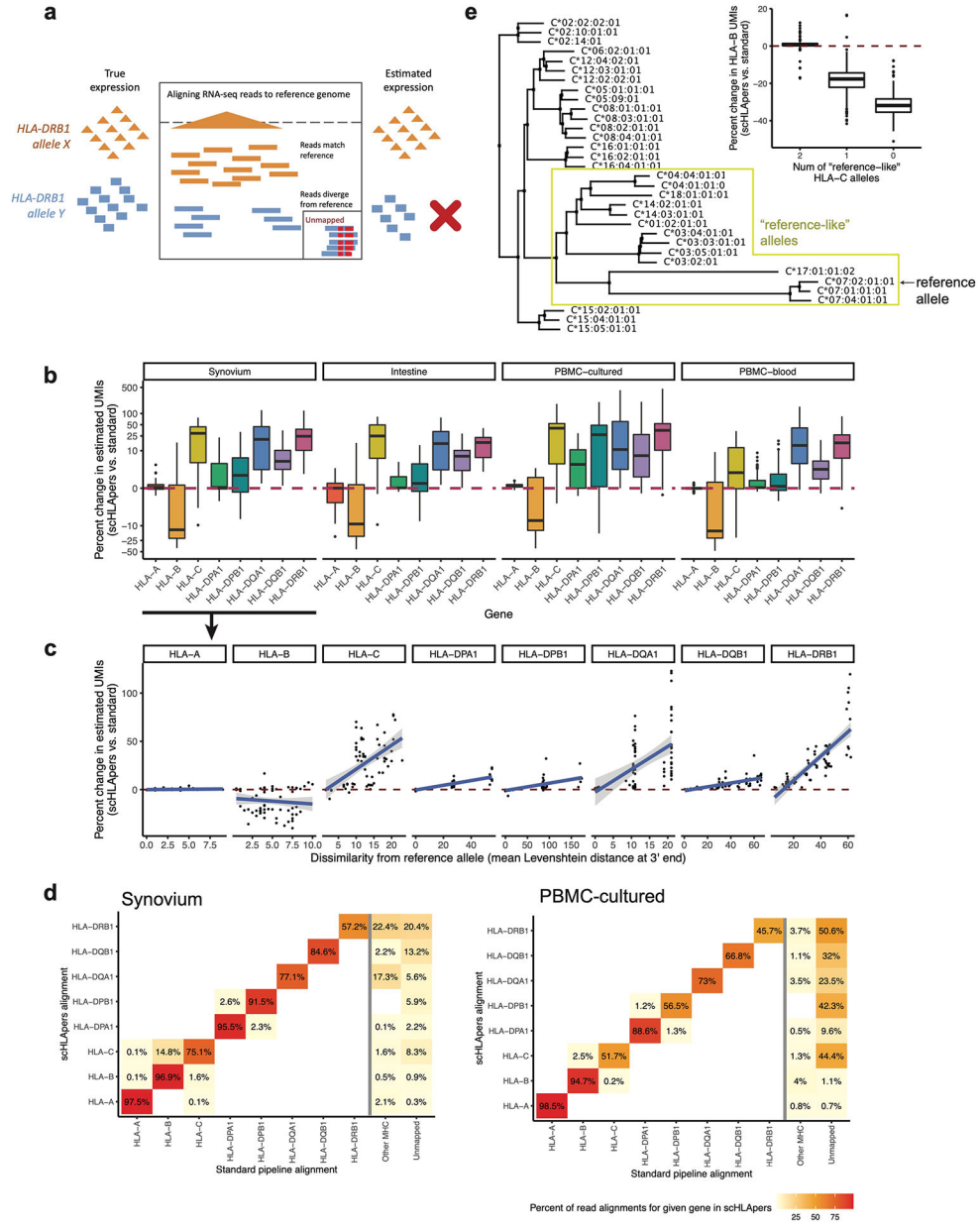
Extended Data Fig. 1 |. Correcting HLA expression estimation bias with scHLApers.
a, Schematic showing how high *HLA* gene polymorphism leads to bias in read alignment to a single reference genome. Consider two hypothetical individuals who are either homozygous for *HLA-DRB1* allele X (orange) or allele Y (blue), where the reference allele is X. Reads from X will align perfectly to the reference, leading to accurate *HLA-DRB1* quantification. However, for Y, reads will fail to align to the reference due to discordant sequence content, leading to unmapped reads and underestimation of expression.

b, Percentage change in expression (total UMIs for *HLA* gene per individual, *y*-axis) across cohorts (synovium, $n = 69$ individuals; intestine, $n = 22$; PBMC-cultured, $n = 73$; PBMC-blood, $n = 909$). **c**, Percentage change in estimated expression (total UMIs for *HLA* gene per individual, *y*-axis) in synovium ($n = 69$) as a function of the mean (between the individual's two alleles) Levenshtein distance relative to the GRCh38 reference allele at the 3' end of each gene (*x*-axis). For **b** and **c**, dashed horizontal red lines denote no change. Fitted linear regression line (blue) shown with 95% confidence region. **d**, Heatmap showing the alignment of reads to each gene in scHLApers (rows) versus where the same read aligned ('came from') in the standard pipeline (columns) for synovium (top) and PBMC-cultured (bottom). Columns include *HLA* genes, other regions in the extended MHC, or unmapped reads. Rows sum to 100%, and a darker color indicates that more of the reads aligning to a given gene in scHLApers came from the corresponding location in the standard pipeline. **e**, Phylogenetic tree derived from a multiple sequence alignment of *HLA-C* allelic genomic sequences. The reference allele is *C*07:02*. Yellow box shows alleles similar to the reference ('reference-like'). Boxplot on right shows the change in *HLA-B* estimated UMI counts summed across cells from each sample (*y*-axis) compared to the genotype for *HLA-C* in terms of dosage of 'reference-like' alleles (*x*-axis), across $n = 1,073$ individuals from all cohorts. For **b** and **e**, boxplot center line represents median, lower/upper box limits represent 25/75% quantiles, whiskers extend to box limit $\pm 1.5 \times$ IQR, and outlying points are plotted individually.
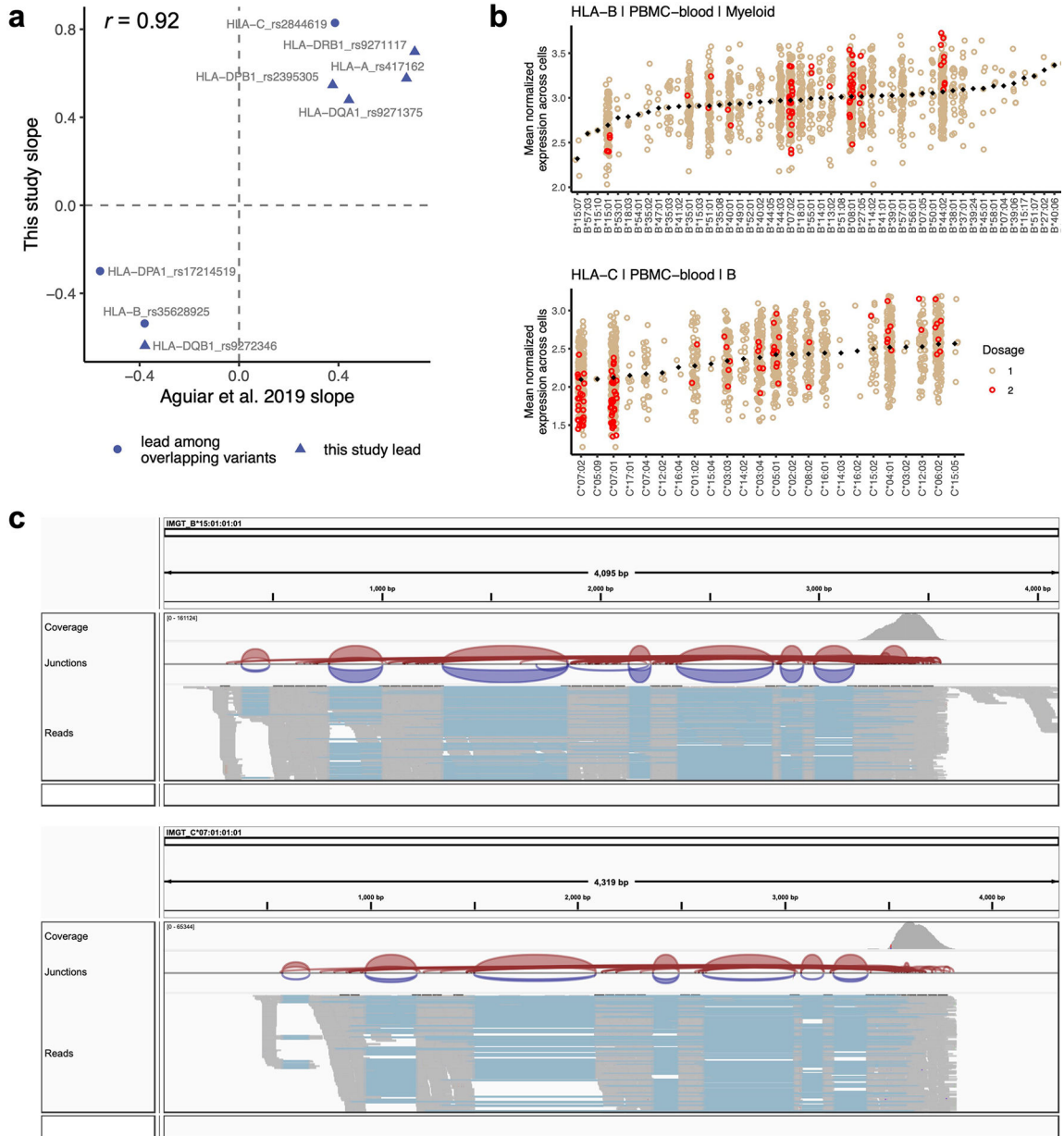
Extended Data Fig. 2 |. Concordance of eQTLs with bulk RNA-seq, differential allelic expression, and read alignment visualization.

a, Concordance between the effect sizes of lead *HLA* eQTLs identified in the multi-cohort pseudobulk model for B cells (this study, *y*-axis) and the same variant's effect in LCLs identified through bulk RNA-seq eQTL analysis (Aguiar et al., *x*-axis). Because not all lead variants in this study were directly comparable due to different sets of tested variants, we tested the concordance of the most significant variant present in both datasets (triangles indicate that the exact lead variant in this study was also tested in Aguiar et al., whereas circles indicate 'substitute' lead variants was used for comparison). **b**, *HLA-B* expression in myeloid cells (top, *n* = 861 individuals) and *HLA-C* expression in B cells (bottom, *n* = 909), showing mean log(CP10k + 1)-normalized expression (*y*-axis) across cells for each individual in PBMC-blood by allele (*x*-axis). Each individual's expression value is plotted

once if they are homozygous (red) and twice if heterozygous (tan) for each allele (imputed dosage is rounded to the nearest integer). The black diamonds show the mean value for each allele (used to order the x-axis). **c**, Integrative Genomics Viewer (IGV) screenshots showing read alignments for alleles *HLA-B*15:01* and *HLA-C*07:01*, associated with lower expression of the respective genes, for a representative individual in synovium.
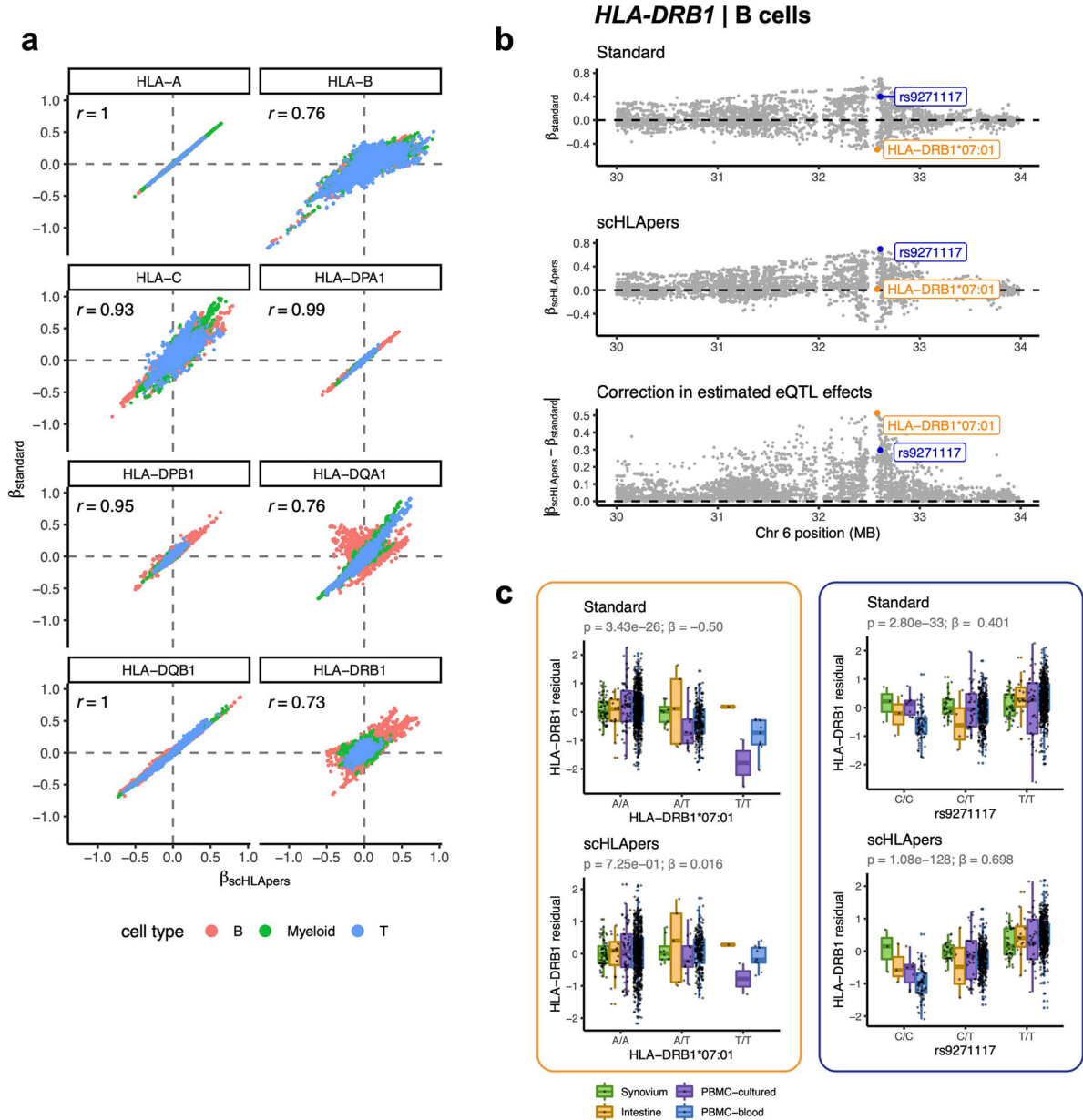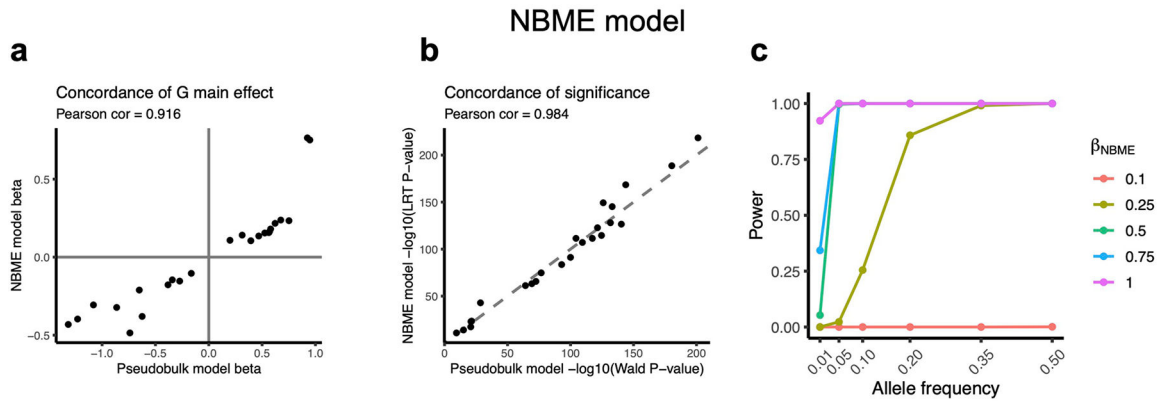

Extended Data Fig. 3 |. Personalization improves eQTL effect size estimates.
a, Comparison of eQTL effect size estimates calculated using expression quantified by scHLApers (*x*-axis) vs. standard pipeline (*y*-axis). Each dot represents one of 12,045 MHC-wide genetic variants tested using the pseudobulk eQTL model per cell type (color). Pearson correlation is labeled for each gene. **b**, Example of eQTL effect correction through the
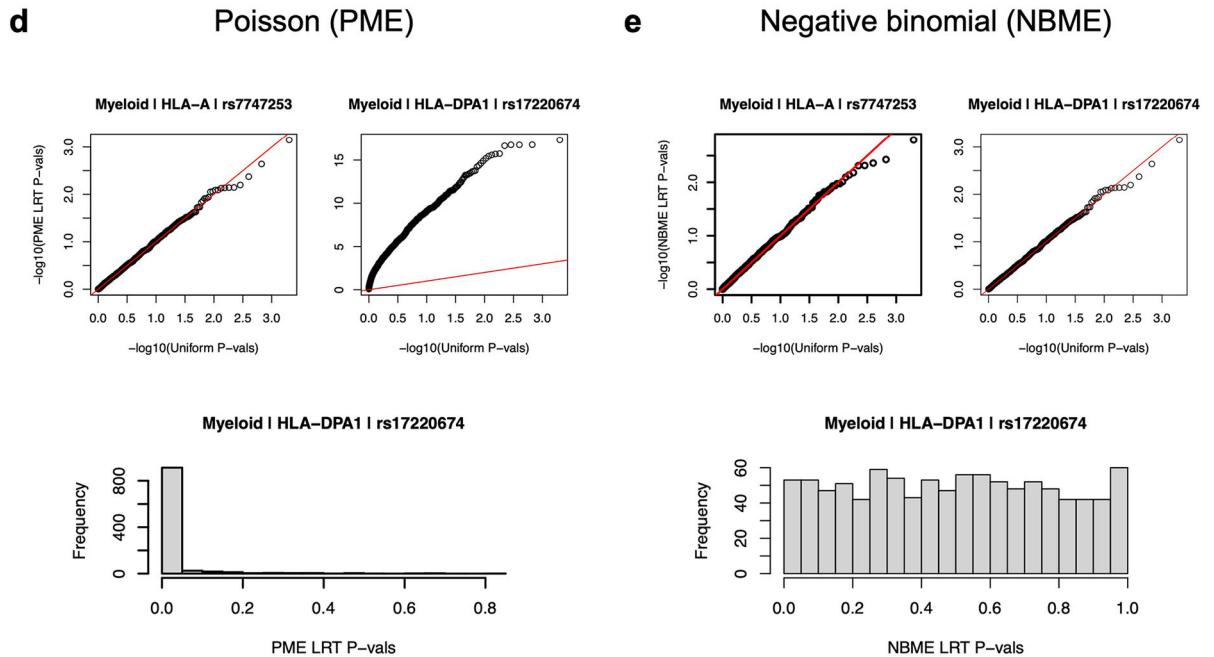
use of corrected expression estimates, shown for *HLA-DRB1* in B cells. eQTL effect sizes (*y*-axis) estimated for MHC variants along Chr. 6 (*x*-axis), shown for standard pipeline (top), scHLApers pipeline (middle), and the magnitude of difference between the betas from the two pipelines (bottom). The variant with the largest correction in estimated eQTL effect (*HLA-DRB1*07:01*) is labeled in orange, and the lead variant in the scHLApers pipeline (rs9271117) is labeled in blue. **c**, Boxplots visualizing the eQTL effects across individuals for *HLA-DRB1*07:01* (left) and rs9271117 (right) using *HLA-DRB1* expression estimates from the standard (top) vs. scHLApers (bottom) pipelines. Increased dosage of the ALT allele (*x*-axis) vs. *HLA-DRB1* expression in B cells (*y*-axis: units are residual of inverse normal transformed mean $\log(CP10k + 1)$-normalized expression across cells after regressing out covariates), across $n = 1{,}069$ individuals total (synovium, $n = 65$; intestine, $n = 22$; PBMC-cultured, $n = 73$; PBMC-blood, $n = 909$), plotted by dataset (color). For *HLA-DRB1*07:01*, 'A' denotes absence of the allele, and 'T' denotes presence (rather than REF/ALT nucleotides). Nominal Wald *P*-values are derived from linear regression (two-sided test).

Testing main effect only (no cell state interaction terms)

NBME model

a Concordance of G main effect
Pearson cor = 0.916

b Concordance of significance
Pearson cor = 0.984

c

Testing cell state interaction under null hypothesis (permuted data)

d Poisson (PME)

e Negative binomial (NBME)

Myeloid | HLA−A | rs7747253

Myeloid | HLA−DPA1 | rs17220674

Myeloid | HLA−A | rs7747253

Myeloid | HLA−DPA1 | rs17220674

Myeloid | HLA−DPA1 | rs17220674

Myeloid | HLA−DPA1 | rs17220674

Extended Data Fig. 4 |. Testing single-cell NBME model for concordance with pseudobulk and for calibration for genotype-cell-state interactions.

a-e, The models in **a-c** test genotype main effects, whereas **d** and **e** test genotype-cell-state interaction. **a,b**, Concordance of genotype main effect estimates (**a**) and significance of genotype main effect (**b**) between the NBME model (*y*-axis) and the pseudobulk model for the PBMC-blood dataset (*x*-axis) across all cell types and classical *HLA* genes. **c**, Power of the NBME single-cell eQTL model to detect regulatory effects across allele frequencies. The proportion of simulations where the null hypothesis was appropriately rejected at $\alpha = 5 \times 10^{-8}$ (*y*-axis) in the presence of a simulated eQTL effect across 1000 simulations. Simulations were run across a range of eQTL allele frequencies (*x*-axis) and effect sizes (colors) using the PBMC-blood myeloid data and *HLA-DQA1* expression. **d,e**, We permuted cell state (10 hPCs as a block) for 1,000 tests and obtained interaction *P*-values from a one-

sided likelihood ratio test (LRT) comparing to the null model without G×hPC interaction terms. Q-Q plots showing statistical calibration (compared to uniform *P*-values) for PME model (**d**) versus NBME model (**e**) when testing for cell state interactions for representative class I (*HLA-A*) and class II (*HLA-DPA1*) genes in myeloid cells in PBMC-blood. The red line is the identity line. The histograms below show distributions of LRT *P*-values for *HLA-DPA1*.

Supplementary Material

Refer to Web version on PubMed Central for supplementary material.

Acknowledgements

Data availability

The GRCh38 reference genome (primary assembly) and Gencode v38 annotation file can be downloaded at https://www.gencodegenes.org/human/release_38.html. For the synovium dataset, the single-cell expression data are available on Synapse at https://doi.org/10.7303/syn52297840. Genotype data are available on the Arthritis and Autoimmune and Related Diseases Knowledge Portal (ARK Portal, https://arkportal.synapse.org/Explore/Datasets/DetailsPage?id=syn52297840). For intestine, the raw scRNA-seq data (bam files) was obtained from the Broad Data Use Oversight System (DUOS) (dataset name: Ulcerative_Colitis_in_Colon_Regev_Xavier); the genotype data are available on dbGaP (phs001642). For PBMC-cultured, the raw scRNA-seq data (FASTQ files) was obtained from GEO (PRJNA682434), and the imputed low-pass WGS data is publicly available at SRA (PRJNA736483) and Zenodo (https://doi.org/10.5281/zenodo.4273999). For PBMC-blood (OneK1K cohort), both the raw scRNA-seq data (bam files) and genotyping data are publicly available on GEO (GSE196830). The reprocessed versions of all scRNA-seq count matrices from this study after realignment with scHLApers are publicly available on Figshare (https://doi.org/10.6084/m9.figshare.24311335).

Code availability

Code and tutorials to run the scHLApers pipeline (v1.0) are available on GitHub (https://github.com/immunogenomics/scHLApers) and Zenodo (https://doi.org/10.5281/zenodo.10003910). Scripts for reproducing analyses in the manuscript are also available on GitHub (https://github.com/immunogenomics/hla2023) and Zenodo (https://doi.org/10.5281/zenodo.10003911).

Accelerating Medicines Partnership Program: Rheumatoid Arthritis and Systemic Lupus Erythematosus (AMP RA/SLE) Network

Jennifer Albrecht[22], William Apruzzese[5], Nirmal Banda[24], Jennifer L. Barnas[22], Joan M. Bathon[25], Ami Ben-Artzi[26], Brendan F. Boyce[27], David L. Boyle[28], S. Louis Bridges Jr.[20,21], Vivian P. Bykerk[20,21], Debbie Campbell[22], Hayley L. Carr[28,29], Arnold Ceponis[30], Adam Chicoine[5], Andrew Cordle[31], Michelle Curtis[1,2,3,4,5], Kevin D. Deane[24], Edward DiCarlo[32], Patrick Dunn[33,34], Andrew Filer[28,29,35], Gary S. Firestein[30], Lindsy Forbess[28], Laura Geraldino-Pardilla[25], Susan M. Goodman[20,21], Ellen M. Gravallese[5], Peter K. Gregersen[36], Joel M. Guthridge[37], V. Michael Holers[24], Diane Horowitz[36], Laura B. Hughes[38], Kazuyoshi Ishigaki[1,2,3,4,5,39], Lionel B. Ivashkiv[20,21], Judith A. James[37], Gregory Keras[5], Ilya Korsunsky[1,2,3,4,5], Amit Lakhanpal[20,21], James A. Lederer[40], Myles Lewis[41,42], Zhihan J. Li[5], Yuhong Li[5], Katherine P. Liao[3,5], Arthur M. Mandelin II[43], Ian Mantel[20,21], Kathryne E. Marks[5], Mark Maybury[28], Andrew McDavid[44], Mandy J. McGeachy[45], Joseph Mears[1,2,3,4,5], Nida Meednu[22], Nghia Millard[1,2,3,4,5], Larry W. Moreland[24,45], Saba Nayar[28,29,35], Alessandra Nerviani[41,42], Dana E. Orange[20,46], Harris Perlman[43], Costantino Pitzalis[41,42,47], Javier Rangel-Moreno[22], Karim Raza[28,29], Yakir Reshef[1,2,3,4,5], Christopher Ritchlin[22], Felice Rivellese[41,42], William H. Robinson[48], Ilfita Sahbudin[28], Anvita Singaraju[20,21], Jennifer A. Seifert[24], Kamil Slowikowski[3,4,49,50], Melanie H. Smith[20], Darren Tabechian[22], Dagmar Scheel-Toellner[28,29], Paul J. Utz[48], Gerald F. M. Watts[5], Kevin Wei[5], Kathryn Weinand[1,2,3,4,5], Dana Weisenfeld[5], Michael H. Weisman[26,48], Aaron Wyse[31], Qian Xiao[1,2,3,4,5] & Zhu Zhu[5]

[24]Division of Rheumatology, University of Colorado School of Medicine, Aurora, CO, USA. [25]Division of Rheumatology, Columbia University College of Physicians and Surgeons, New York, NY, USA. [26]Division of Rheumatology, Cedars-Sinai Medical Center, Los Angeles, CA, USA. [27]Department of Pathology and Laboratory Medicine, University of Rochester Medical Center, Rochester, NY, USA. [28]Rheumatology Research Group, Institute for Inflammation and Ageing, University of Birmingham, Birmingham, UK. [29]NIHR Birmingham Biomedical Research Center and Clinical Research Facility, University of Birmingham, Queen Elizabeth Hospital, Birmingham, UK. [30]Division of Rheumatology, Allergy and Immunology, University of California, San Diego, La Jolla, CA, USA. [31]Department of Radiology, University of Pittsburgh Medical Center, Pittsburgh, PA, USA. [32]Department of Pathology and Laboratory Medicine, Hospital for Special Surgery, New York, NY, USA. [33]Division of Allergy, Immunology, and Transplantation, National Institute of Allergy and Infectious Diseases, National Institutes of Health, Bethesda, MD, USA. [34]Northrop Grumman Health Solutions, Rockville, MD, USA. [35]Birmingham Tissue Analytics, Institute of Translational Medicine, University of Birmingham, Birmingham, UK. [36]Feinstein Institute for Medical Research, Northwell Health, Manhasset, New York, NY, USA. [37]Department of Arthritis & Clinical Immunology, Oklahoma Medical Research Foundation, Oklahoma City, OK, USA. [38]Division of Clinical Immunology and Rheumatology, Department of Medicine, University of Alabama at Birmingham, Birmingham, AL, USA. [39]Laboratory for Human Immunogenetics, RIKEN Center for Integrative Medical Sciences, Yokohama, Japan. [40]Department of Surgery, Brigham and Women's Hospital and Harvard Medical School, Boston, MA, USA. [41]Centre

for Experimental Medicine & Rheumatology, William Harvey Research Institute, Queen Mary University of London, London, UK. [42]Barts Health NHS Trust, Barts Biomedical Research Centre, National Institute for Health and Care Research, London, UK. [43]Division of Rheumatology, Department of Medicine, Northwestern University Feinberg School of Medicine, Chicago, IL, USA. [44]Department of Biostatistics and Computational Biology, University of Rochester School of Medicine and Dentistry, Rochester, NY, USA. [45]Division of Rheumatology and Clinical Immunology, University of Pittsburgh School of Medicine, Pittsburgh, PA, USA. [46]Laboratory of Molecular Neuro-Oncology, The Rockefeller University, New York, NY, USA. [47]Department of Biomedical Sciences, Humanitas University and Humanitas Research Hospital, Milan, Italy. [48]Division of Immunology and Rheumatology, Institute for Immunity, Transplantation and Infection, Stanford University School of Medicine, Stanford, CA, USA. [49]Center for Immunology and Inflammatory Diseases, Department of Medicine, Massachusetts General Hospital, Boston, MA, USA. [50]MGH Cancer Center, Boston, MA, USA.

References

1. Lenz TL, Spirin V, Jordan DM & Sunyaev SR Excess of deleterious mutations around HLA genes reveals evolutionary cost of balancing selection. Mol. Biol. Evol 33, 2555–2564 (2016). [PubMed: 27436009]

2. Dendrou CA, Petersen J, Rossjohn J & Fugger L HLA variation and disease. Nat. Rev. Immunol 18, 325–339 (2018). [PubMed: 29292391]

3. Matzaraki V, Kumar V, Wijmenga C & Zhernakova A The MHC locus and genetic susceptibility to autoimmune and infectious diseases. Genome Biol. 18, 76 (2017). [PubMed: 28449694]

4. Trowsdale J & Knight JC Major histocompatibility complex genomics and human disease. Annu. Rev. Genomics Hum. Genet 14, 301–323 (2013). [PubMed: 23875801]

5. Okada Y. et al. Fine mapping major histocompatibility complex associations in psoriasis and its clinical subtypes. Am. J. Hum. Genet 95, 162–172 (2014). [PubMed: 25087609]

6. Raychaudhuri S. et al. Five amino acids in three HLA proteins explain most of the association between MHC and seropositive rheumatoid arthritis. Nat. Genet 44, 291–296 (2012). [PubMed: 22286218]

7. Hollenbach JA & Oksenberg JR The immunogenetics of multiple sclerosis: a comprehensive review. J. Autoimmun 64, 13–25 (2015). [PubMed: 26142251]

8. Vader W. et al. The HLA-DQ2 gene dose effect in celiac disease is directly related to the magnitude and breadth of gluten-specific T cell responses. Proc. Natl Acad. Sci. USA 100, 12390–12395 (2003). [PubMed: 14530392]

9. Hu X. et al. Additive and interaction effects at three amino acid positions in HLA-DQ and HLA-DR molecules drive type 1 diabetes risk. Nat. Genet 47, 898–905 (2015). [PubMed: 26168013]

10. Ishigaki K. et al. HLA autoimmune risk alleles restrict the hypervariable region of T cell receptors. Nat. Genet 54,393–402 (2022). [PubMed: 35332318]

11. Sharon E. et al. Genetic variation in MHC proteins is associated with T cell receptor expression biases. Nat. Genet 48, 995–1002 (2016). [PubMed: 27479906]

12. Broughton SE et al. Biased T cell receptor usage directed against human leukocyte antigen DQ8-restricted gliadin peptides is associated with celiac disease. Immunity 37, 611–621 (2012). [PubMed: 23063329]

13. Apps R. et al. Influence of HLA-C expression level on HIV control. Science 340, 87–91 (2013). [PubMed: 23559252]

14. Cavalli G. et al. MHC class II super-enhancer increases surface expression of HLA-DR and HLA-DQ and affects cytokine production in autoimmune vitiligo. Proc. Natl Acad. Sci. USA 113, 1363–1368 (2016). [PubMed: 26787888]

15. Raj P. et al. Regulatory polymorphisms modulate the expression of HLA class II molecules and promote autoimmunity. eLife 5, e12089 (2016). [PubMed: 26880555]

16. D'Antonio M. et al. Systematic genetic analysis of the MHC region reveals mechanistic underpinnings of HLA type associations with disease. eLife 8, e48476 (2019). [PubMed: 31746734]

17. Aguiar VRC, César J, Delaneau O, Dermitzakis ET & Meyer D Expression estimation and eQTL mapping for HLA genes with a personalized pipeline. PLoS Genet. 15, e1008091 (2019). [PubMed: 31009447]

18. Gutierrez-Arcelus M. et al. Allele-specific expression changes dynamically during T cell activation in HLA and other autoimmune loci. Nat. Genet 52, 247–253 (2020). [PubMed: 32066938]

19. Nathan A. et al. Single-cell eQTL models reveal dynamic T cell state dependence of disease loci. Nature 606, 120–128 (2022). [PubMed: 35545678]

20. Cuomo ASE et al. CellRegMap: a statistical framework for mapping context-specific regulatory variants using scRNA-seq. Mol. Syst. Biol 18, e10663 (2022). [PubMed: 35972065]

21. Schmiedel BJ et al. Single-cell eQTL analysis of activated T cell subsets reveals activation and cell type–dependent effects of disease-risk variants. Sci. Immunol 7, eabm2508 (2022). [PubMed: 35213211]

22. Meyer D, Aguiar VRC, Bitarello BD, Brandt DYC & Nunes K A genomic perspective on HLA evolution. Immunogenetics 70, 5–27 (2018). [PubMed: 28687858]

23. Brandt DYC et al. Mapping bias overestimates reference allele frequencies at the HLA genes in the 1000 Genomes Project Phase I data. G3 5, 931–941 (2015). [PubMed: 25787242]

24. Sakaue S. et al. A statistical genetics guide to identifying HLA alleles driving complex disease. Nat. Protoc 18, 2625–2641 (2023). [PubMed: 37495751]

25. Aguiar VRC, Masotti C, Camargo AA & Meyer D HLApers: HLA typing and quantification of expression with personalized index. Methods Mol. Biol 2120, 101–112 (2020). [PubMed: 32124314]

26. Bettens F. et al. Regulation of HLA class I expression by non-coding gene variations. PLoS Genet. 18, e1010212 (2022). [PubMed: 35666741]

27. Robinson J. et al. IPD-IMGT/HLA database. Nucleic Acids Res. 48, D948–D955 (2020). [PubMed: 31667505]

28. Kaminow B, Yunusov D & Dobin A STARsolo: accurate, fast and versatile mapping/quantification of single-cell and single-nucleus RNA-seq data. Preprint at bioRxiv 10.1101/2021.05.05.442755 (2021).

29. Zhang F et al. Deconstruction of rheumatoid arthritis synovium defines inflammatory subtypes. Nature 10.1038/s41586-023-06708-y (2023).

30. Smillie CS et al. Intra- and inter-cellular rewiring of the human colon during ulcerative colitis. Cell 178, 714–730.e22 (2019). [PubMed: 31348891]

31. Randolph HE et al. Genetic ancestry effects on the response to viral infection are pervasive but cell type specific. Science 374, 1127–1133 (2021). [PubMed: 34822289]

32. Yazar S. et al. Single-cell eQTL mapping identifies cell type-specific genetic control of autoimmune disease. Science 376, eabf3041 (2022). [PubMed: 35389779]

33. Jia X. et al. Imputing amino acid polymorphisms in human leukocyte antigens. PLoS ONE 8, e64683 (2013). [PubMed: 23762245]

34. Luo Y. et al. A high-resolution HLA reference panel capturing global population diversity enables multi-ancestry fine-mapping in HIV host response. Nat. Genet 53, 1504–1516 (2021). [PubMed: 34611364]

35. Dunlap G. et al. Clonal associations of lymphocyte subsets and functional states revealed by single cell antigen receptor profiling of T and B cells in rheumatoid arthritis synovium. Preprint at bioRxiv 10.1101/2023.03.18.533282 (2023).

36. Wang Z. et al. Clonally diverse CD38+HLA-DR+CD8+ T cells persist during fatal H7N9 disease. Nat. Commun 9, 824 (2018). [PubMed: 29483513]

37. Tippalagama R. et al. HLA-DR marks recently divided antigen-specific effector CD4 T cells in active tuberculosis patients. J. Immunol 207, 523–533 (2021). [PubMed: 34193602]

38. Soskic B. et al. Immune disease risk variants regulate gene expression dynamics during CD4^{+} T cell activation. Nat. Genet 54, 817–826 (2022). [PubMed: 35618845]

39. Holling TM, Schooten E & van Den Elsen PJ Function and regulation of MHC class II molecules in T-lymphocytes: of mice and men. Hum. Immunol 65, 282–290 (2004). [PubMed: 15120183]

40. LaSalle JM, Tolentino PJ, Freeman GJ, Nadler LM & Hafler DA Early signaling defects in human T cells anergized by T cell presentation of autoantigen. J. Exp. Med 176, 177–186 (1992). [PubMed: 1535366]

41. Lanzavecchia A, Roosnek E, Gregory T, Berman P & Abrignani S T cells can present antigens such as HIV gp120 targeted to their own surface molecules. Nature 334, 530–532 (1988). [PubMed: 2841610]

42. Hagopian W. et al. Co-occurrence of type 1 diabetes and celiac disease autoimmunity. Pediatrics 140, e20171305 (2017). [PubMed: 29018046]

43. Yamamoto F. et al. Capturing differential allele-level expression and genotypes of all classical HLA loci and haplotypes by a new capture RNA-seq method. Front. Immunol 11, 941 (2020). [PubMed: 32547543]

44. Kaur G. et al. Structural and regulatory diversity shape HLA-C protein expression levels. Nat. Commun 8, 15924 (2017). [PubMed: 28649982]

45. Kulkarni S. et al. Genetic interplay between HLA-C and MIR148A in HIV control and Crohn disease. Proc. Natl Acad. Sci. USA 110, 20705–20710 (2013). [PubMed: 24248364]

46. Chandran V. et al. Killer-cell immunoglobulin-like receptor gene polymorphisms and susceptibility to psoriatic arthritis. Rheumatology 53, 233–239 (2014). [PubMed: 24185760]

47. Ota M. et al. Dynamic landscape of immune cell-specific gene regulation in immune-mediated diseases. Cell 184, 3006–3021. e17 (2021). [PubMed: 33930287]

48. Korsunsky I. et al. Fast, sensitive and accurate integration of single-cell data with Harmony. Nat. Methods 16, 1289–1296 (2019). [PubMed: 31740819]

49. Kang JB et al. Efficient and precise single-cell reference atlas mapping with Symphony. Nat. Commun 12, 5890 (2021). [PubMed: 34620862]

50. Wilkinson ST et al. Partial plasma cell differentiation as a mechanism of lost major histocompatibility complex class II expression in diffuse large B-cell lymphoma. Blood 119, 1459–1467 (2012). [PubMed: 22167754]

51. Yoon HS et al. ZBTB32 is an early repressor of the CIITA and MHC class II gene expression during B cell differentiation to plasma cells. J. Immunol 189, 2393–2403 (2012). [PubMed: 22851713]

52. Kumasaka N. et al. Mapping interindividual dynamics of innate immune response at single-cell resolution. Nat. Genet 55, 1066–1075 (2023). [PubMed: 37308670]

53. Kang JB, Raveane A, Nathan A, Soranzo N & Raychaudhuri S Methods and insights from single-cell expression quantitative trait loci. Annu. Rev. Genomics Hum. Genet 24, 277–303 (2023). [PubMed: 37196361]

54. Yao C. et al. Sex- and age-interacting eQTLs in human complex diseases. Hum. Mol. Genet 23, 1947–1956 (2014). [PubMed: 24242183]

55. Davenport EE et al. Discovering in vivo cytokine-eQTL interactions from a lupus clinical trial. Genome Biol. 19, 168 (2018). [PubMed: 30340504]

56. Zhernakova DV et al. Identification of context-dependent expression quantitative trait loci in whole blood. Nat. Genet 49, 139–145 (2017). [PubMed: 27918533]

57. Calzetti F. et al. Human dendritic cell subset 4 (DC4) correlates to a subset of CD14[dim/−]CD16++ monocytes. J. Allergy Clin. Immunol 141, 2276–2279.e3 (2018). [PubMed: 29366702]

58. Janeway CA, Travers P, Walport M & Shlomchik MJ Immunobiology (CRC Press, 2001).

59. Kambayashi T & Laufer TM Atypical MHC class II-expressing antigen-presenting cells: can anything replace a dendritic cell? Nat. Rev. Immunol 14, 719–730 (2014). [PubMed: 25324123]

60. Prugnolle F. et al. Pathogen-driven selection and worldwide HLA class I diversity. Curr. Biol 15, 1022–1027 (2005). [PubMed: 15936272]

61. Yeung H-Y & Dendrou CA Pregnancy immunogenetics and genomics: implications for pregnancy-related complications and autoimmune disease. Annu. Rev. Genomics Hum. Genet 20, 73–97 (2019). [PubMed: 30848957]

62. Barreiro LB & Quintana-Murci L From evolutionary genetics to human immunology: how selection shapes host defence genes. Nat. Rev. Genet 11, 17–30 (2010). [PubMed: 19953080]

63. Petersdorf EW et al. HLA-C expression levels define permissible mismatches in hematopoietic cell transplantation. Blood 124, 3996–4003 (2014). [PubMed: 25323824]

64. Chowell D. et al. Patient HLA class I genotype influences cancer response to checkpoint blockade immunotherapy. Science 359, 582–587 (2018). [PubMed: 29217585]

65. Naranbhai V. et al. HLA-A*03 and response to immune checkpoint blockade in cancer: an epidemiological biomarker study. Lancet Oncol. 23, 172–184 (2022). [PubMed: 34895481]

66. Matern BM et al. Long-read nanopore sequencing validated for human leukocyte antigen class I typing in routine diagnostics. J. Mol. Diagn 22, 912–919 (2020). [PubMed: 32302780]

67. Liu C. et al. High-resolution HLA typing by long reads from the R10.3 Oxford nanopore flow cells. Hum. Immunol 82, 288–295 (2021). [PubMed: 33612390]

68. Giambartolomei C. et al. Bayesian test for colocalisation between pairs of genetic association studies using summary statistics. PLoS Genet. 10, e1004383 (2014). [PubMed: 24830394]

69. Wallace C. A more accurate method for colocalisation analysis allowing for multiple causal variants. PLoS Genet. 17, e1009440 (2021). [PubMed: 34587156]

70. van der Wijst M. et al. The single-cell eQTLGen consortium. eLife 9, e52155 (2020). [PubMed: 32149610]

71. scHLApers. GitHub. https://github.com/immunogenomics/scHLApers (2023).

72. IMGTHLA. GitHub. https://github.com/ANHIG/IMGTHLA (2023).

73. hlaseqlib. GitHub. https://github.com/genevol-usp/hlaseqlib (2022).

74. tutorial_HLAQCImputation.ipynb. GitHub. https://github.com/immunogenomics/HLA_analyses_tutorial/blob/main/tutorial_HLAQCImputation.ipynb (2023).

75. SNP2HLA.py. GitHub. https://github.com/immunogenomics/HLA_analyses_tutorial/blob/main/scripts/SNP2HLA.py (2023).

76. Chain file for hg19 to hg38 liftover. UCSC. http://hgdownload.soe.ucsc.edu/goldenPath/hg19/liftOver/hg19ToHg38.over.chain.gz (2013).

77. Darby CA, Stubbington MJT, Marks PJ, Martínez Barrio Á & Fiddes IT scHLAcount: allele-specific HLA expression from single-cell gene expression data. Bioinformatics 36, 3905–3906 (2020). [PubMed: 32330223]

78. Azimuth. HuBMAP Consortium. https://app.azimuth.hubmapconsortium.org/app/human-pbmc (2020).

79. Cuomo ASE et al. Optimizing expression quantitative trait locus mapping workflows for single-cell studies. Genome Biol. 22, 188 (2021). [PubMed: 34167583]

80. Stegle O, Parts L, Piipari M, Winn J & Durbin R Using probabilistic estimation of expression residuals (PEER) to obtain increased power and interpretability of gene expression analyses. Nat. Protoc 7, 500–507 (2012). [PubMed: 22343431]

81. Nakagawa S, Johnson PCD & Schielzeth H The coefficient of determination R^2 and intra-class correlation coefficient from generalized linear mixed-effects models revisited and expanded. J. R. Soc. Interface 14, 20170213 (2017). [PubMed: 28904005]
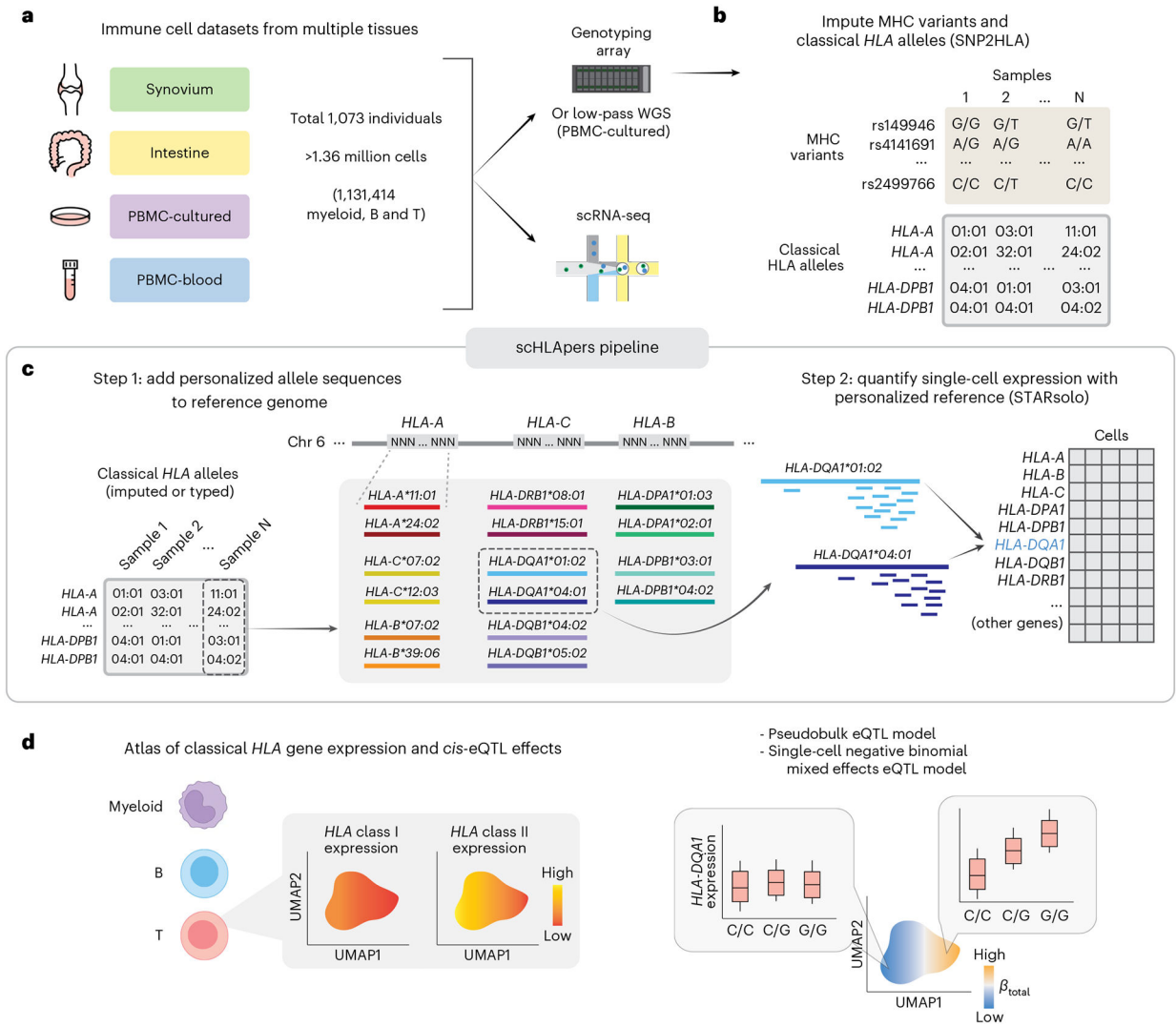
Fig. 1 |. Overview of study and scHLApers pipeline.
a, We used four datasets with genotype and scRNA-seq data: synovium ($n = 69$ individuals, $m = 275,323$ cells), intestine ($n = 22$, $m = 137,321$), PBMC-cultured ($n = 73$, $m = 188,507$), and PBMC-blood ($n = 909$, $m = 765,079$). **b,** Using the genotype data, we imputed SNPs within the MHC and one- and two-field classical *HLA* alleles. **c,** Schematic of scHLApers pipeline, where scRNA-seq reads are aligned to a personalized reference for each individual based on classical *HLA* alleles. In the example, an individual is heterozygous for all eight *HLA* genes, so 16 additional contigs are added to the reference. Original reference gene sequences are masked with Ns. scHLApers outputs a whole-transcriptome counts matrix with improved *HLA* gene estimates. Both alleles contribute to count estimation for each gene. **d,** We generated an atlas of *HLA* expression across all cell types (left) and mapped eQTLs for *HLA* genes in myeloid, B and T cells. Schematic of example dynamic eQTL (right), where eQTL strength (slope, β_{total}) changes across T cell states.
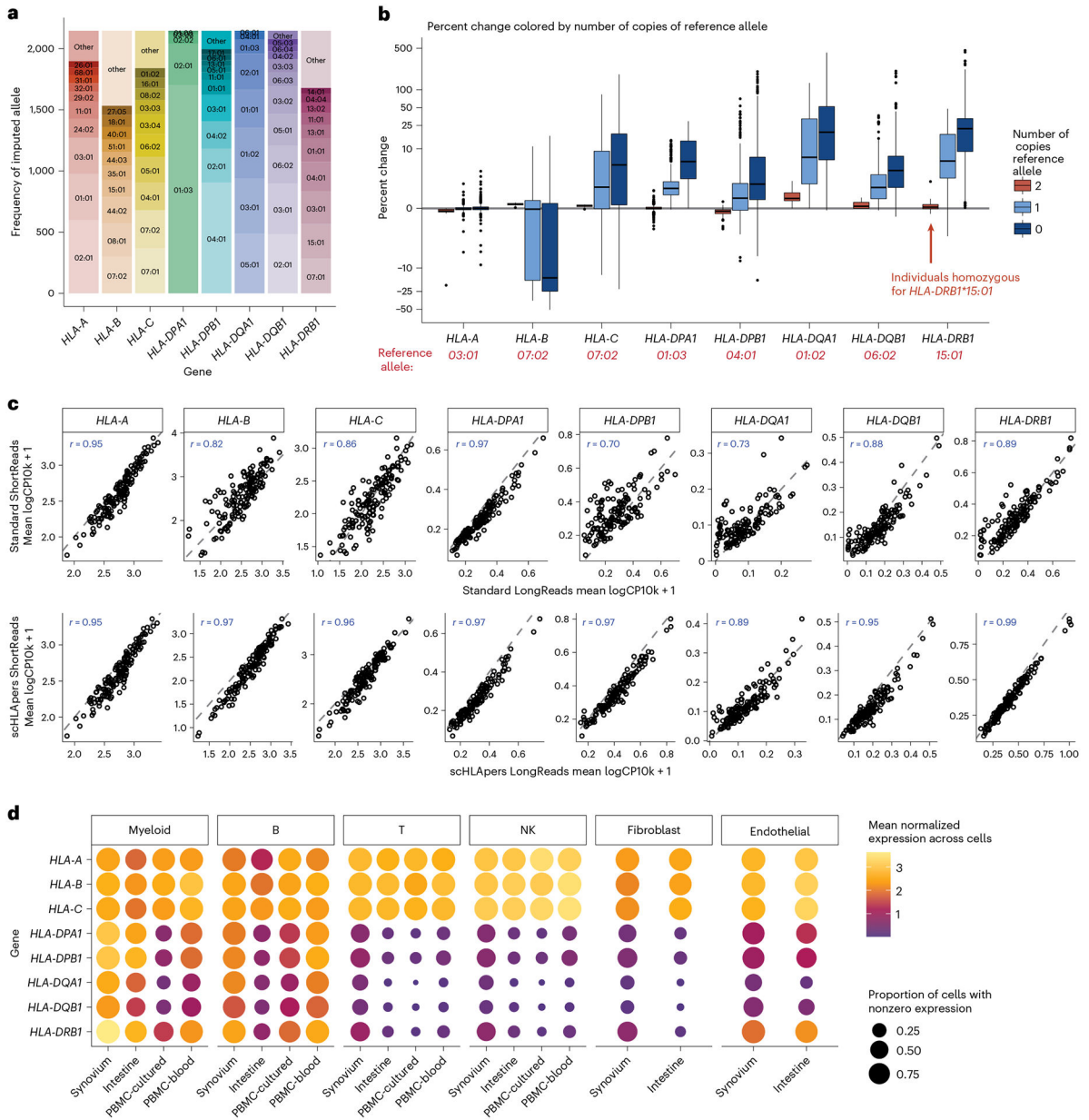
Fig. 2 |. Quantifying single-cell *HLA* expression using scHLApers.

a, Frequency of each imputed two-field *HLA* allele across all cohorts. Most common alleles (up to ten) labeled for each gene, with other alleles grouped into 'other'. Alleles with frequency of less than five are not labeled. **b**, Boxplot (each observation is one sample) showing percentage change (*y* axis) in the estimated UMIs for each *HLA* gene (*x* axis) summed across all cells after quantification with scHLApers (compared to a pipeline using the standard reference genome) in the combined dataset (*n* = 1,073 individuals), colored by number of copies of the reference allele (labeled in red below for each gene). Gray horizontal line denotes no change. Boxplot center line represents median, lower/upper box limits represent 25/75% quantiles, whiskers extend to box limit ± 1.5× interquartile range, and outlying points are plotted individually. **c**, Comparing the estimated *HLA* expression

as measured using shorter reads (84 bp, y axis) versus longer reads (289 bp, x axis) in the standard pipeline (top row) compared to scHLApers (bottom row). Each dot shows the mean log(CP10k + 1)-normalized expression across cells for one sample in PBMC-cultured ($n =$ 146 samples from 73 individuals). r is Pearson correlation; dashed gray line is identity line. **d**, *HLA* expression in different cell types across cohorts: myeloid ($m =$ 145,090 cells), B ($m =$ 180,935), T ($m =$ 805,389), NK ($m =$ 125,865), fibroblasts ($m =$ 82,651) and endothelial ($m =$ 26,300). Dot size indicates proportion of cells with nonzero expression; color indicates log(CP10k + 1)-normalized expression (mean across cells).
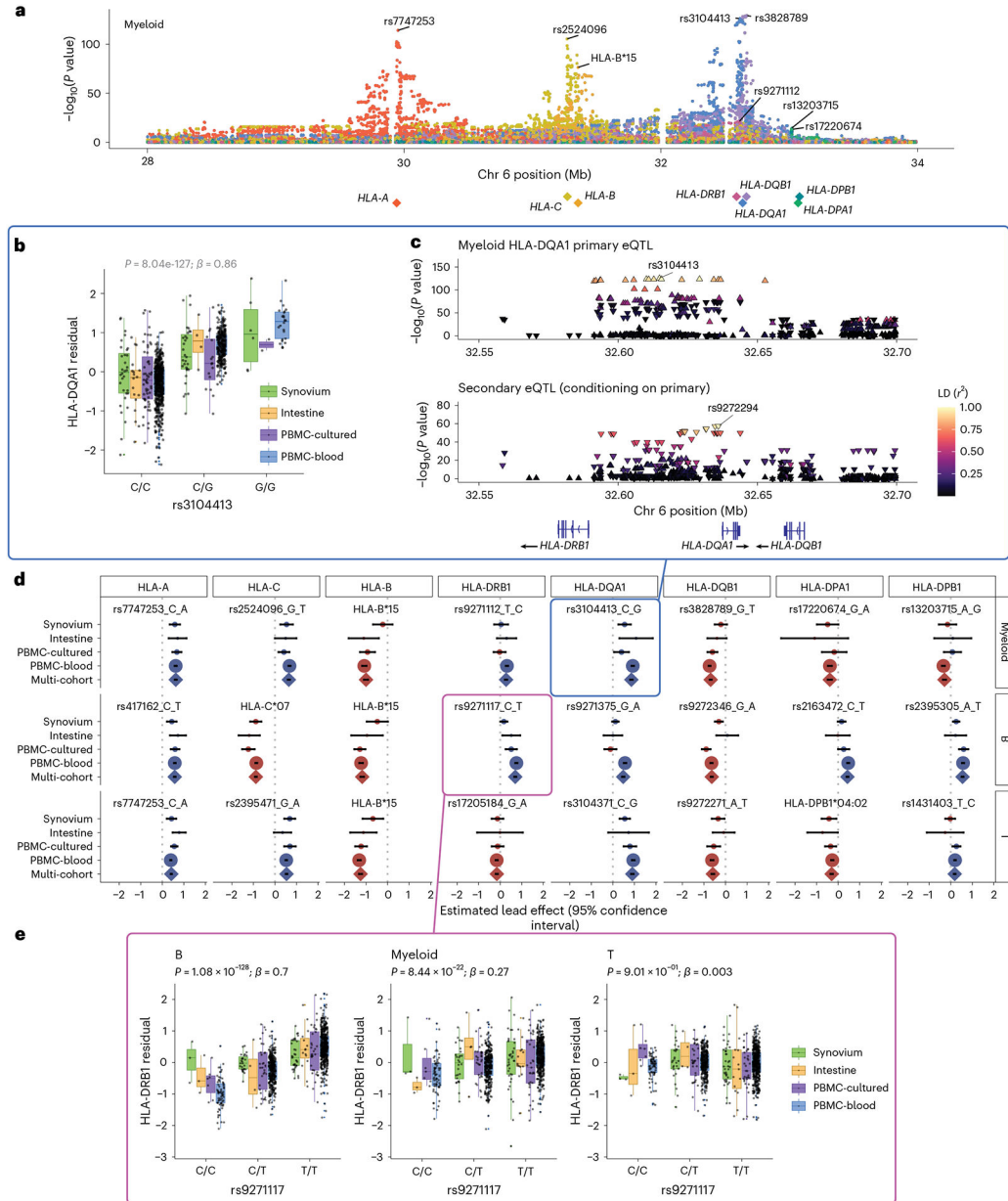
Fig. 3 |. eQTLs for classical *HLA* genes from pseudobulk analysis.

a, Manhattan plot showing the significance (*y* axis) of association between tested MHC variants (*x* axis) and expression of each *HLA* gene (color) in myeloid cells from the multi-cohort model. Most significant (lead) eQTLs are labeled. Diamonds indicate TSS of each gene. **b**, Boxplot showing an example lead eQTL (rs3104413). Increased dosage of the G allele (*x* axis) associates with higher *HLA-DQA1* expression in myeloid cells (*y* axis: units are the residual of inverse normal transformed mean log(CP10k + 1)-normalized expression across cells after regressing out covariates), *n* = 1,025 individuals total (synovium *n* = 69, intestine *n* = 22, PBMC-cultured *n* = 73, PBMC-blood *n* = 861), plotted by dataset (color). All lead eQTLs shown in Supplementary Fig. 6c, Locus zoom plot for the primary (rs3104413) and secondary (rs9272294) eQTLs for *HLA-DQA1* in myeloid

cells. Significance of association (y axis) is shown for nearby variants on chromosome 6 (x axis); color denotes LD (r^2 with lead eQTL in multi-ancestry HLA reference). Triangles point upwards for a positive (downwards for negative) effect on expression. Gene bodies and direction of transcription (arrows) for *HLA-DRB1, HLA-DQA1* and *HLA-DQB1* are underneath. **d**, Grid showing lead eQTLs for each *HLA* gene (columns) in each cell type (rows: myeloid cells $n = 1,025$, B cells $n = 1,069$, and T cells $n = 1,072$ individuals total; for dataset breakdown, see Supplementary Table 2). Each element of the grid includes a forest plot with the estimated lead effect size (x axis) and 95% confidence interval (mean ± 1.96 standard error) of the estimate from the multi-cohort analysis (diamond) and the same variant-gene pair tested for an association within each cohort separately (dots above). Size of the dots/diamond indicates cohort size; color indicates sign of the ALT allele's effect on expression (blue for positive, red for negative). The eQTLs boxed in blue and magenta are highlighted in **b** and **c** and in **e**, respectively. **e**, Example of a cell-type-dependent eQTL (rs9271117) that was the lead eQTL for *HLA-DRB1* and strongest in B cells. Boxplots are formatted analogously to **b** and show the eQTL's effect for all three cell types separately. In **a–c** and **e**, nominal Wald P values are derived from linear regression (two-sided test).
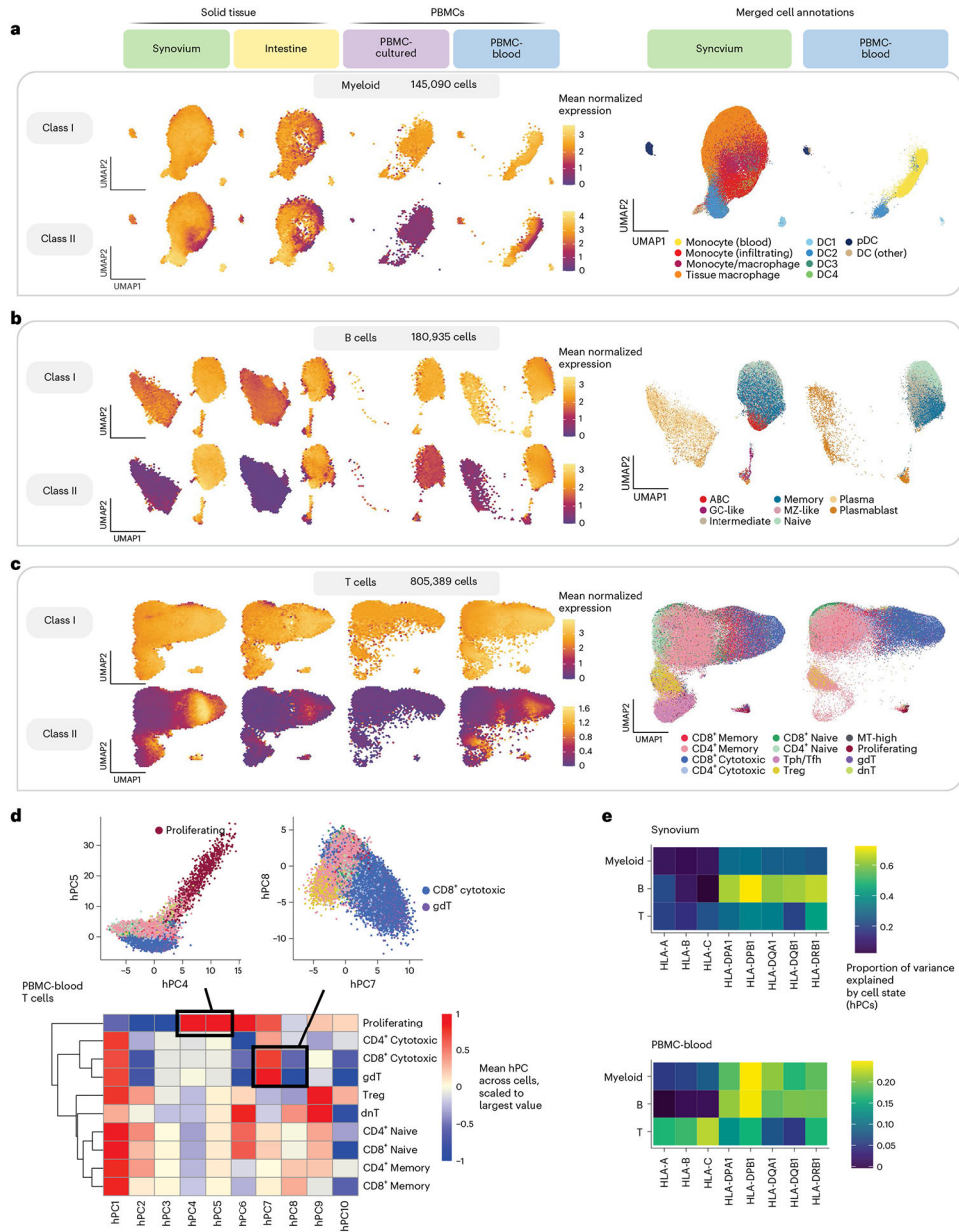
Fig. 4 |. Integrating single cells into a unified cell state embedding across datasets.
a–c, UMAP of cells generated using tissue-defined embedding (top ten hPCs from synovium
and intestine), with PBMC datasets projected into the same space. The plot is divided into
three sections: myeloid cells (**a**), B cells (**b**) and T cells (**c**). Left: class I and II *HLA*
expression across cells across datasets. Cells are binned into hexagons to avoid overplotting
(50 bins per horizontal and vertical UMAP directions) and colored by mean log(CP10k
+ 1)-normalized expression of class I/II genes per bin (for example, for class I, mean
of *HLA-A, HLA-B* and *HLA-C*). Right: cell state annotations (color) for a representative
PBMC (PBMC-blood) and solid tissue (synovium) dataset from merging annotations from
each dataset to a shared set of labels. **d**, Heatmap showing mean value for each hPC (color)
across cells for each discrete cell annotation within T cells in PBMC-blood. Values are

scaled relative to the most extreme value across cell states. Black boxes and inset figures above show examples of how hPCs are linked to original cell state labels: proliferating cells (high in hPC4 and hPC5) and CD8$^+$ cytotoxic and γδ (gdT) cells (high in hPC7, low in hPC8). **e**, Estimated proportion of variance in UMIs explained by cell state hPCs (color) across *HLA* genes and cell types.
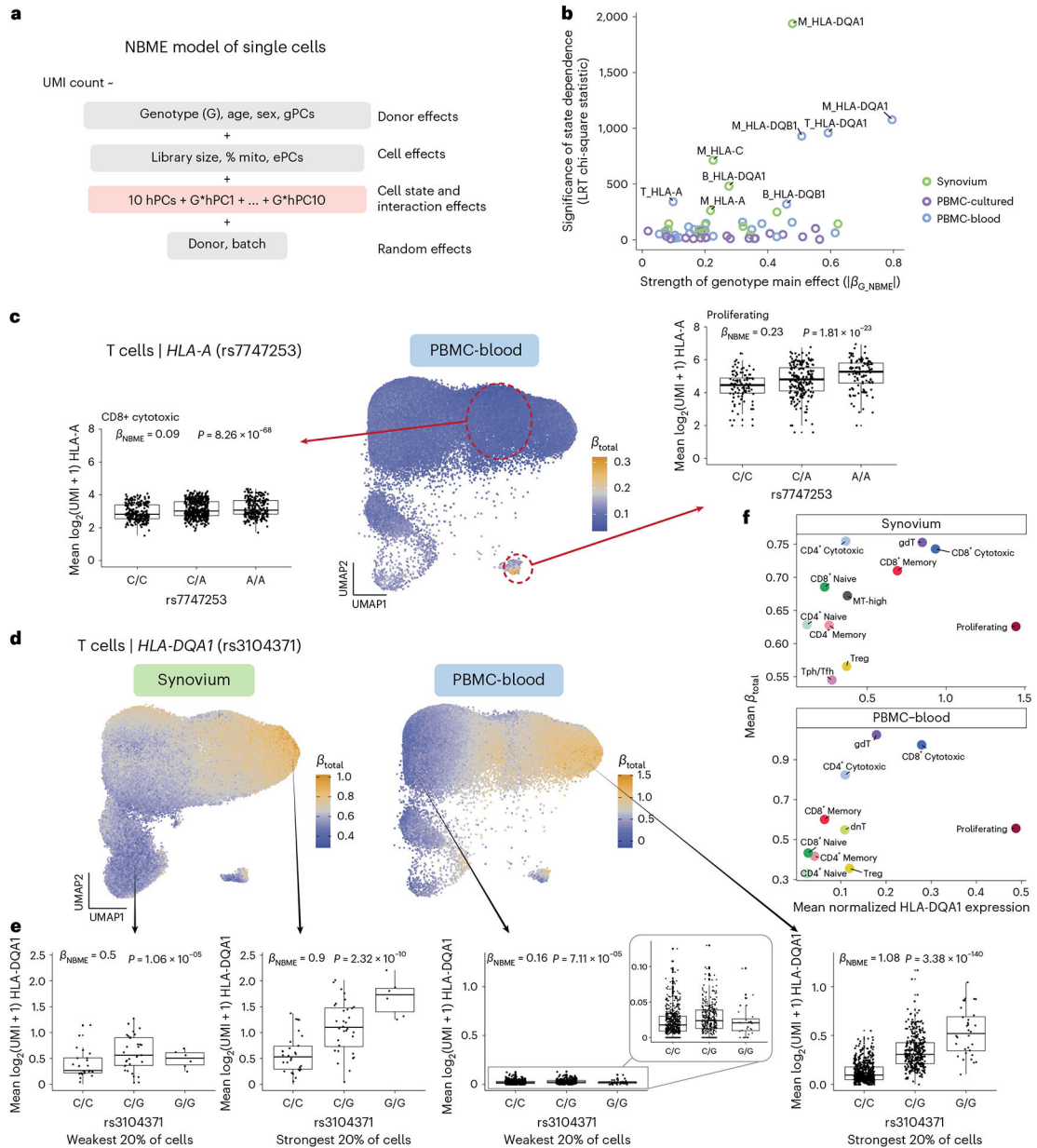
**Fig. 5 |. Identifying dynamic eQTLs by modeling single cells.**
a, NBME model of single cells used to identify cell-state-dependent regulatory effects. Pink box highlights terms for cell state (ten hPCs per cell type) and their interaction with genotype. **b**, Testing lead eQTLs identified in multi-cohort pseudobulk analysis for cell-state dependence using the NBME model in each dataset (color) in myeloid ('M'), B and T cells. Magnitude of genotype main effect (x axis) versus the significance of cell-state interaction (y axis), measured using chi-square (χ^2) statistic from LRT comparing full model (**a**) to null model without G × hPC interactions. **c**, Dynamic *HLA-A* eQTL (rs7747253) in T cells ($n = 909$ individuals, $m = 538,579$ cells in PBMC-blood). UMAP shows T cells colored by estimated eQTL strength (β_{total}). Boxplots for the eQTL effect are shown for two annotated cell states (CD8$^+$ cytotoxic and proliferating, outlined in red circles), showing

mean $\log_2(\text{UMI} + 1)$ of *HLA-A* across all cells in the cell state per individual by genotype. β_{NBME} and *P* values are derived from fitting the NBME model without cell-state interaction terms on the discrete cell populations and comparing to a null model without genotype using an LRT ($n = 908$ individuals, $m = 96{,}516$ cells for CD8^+ cytotoxic; $n = 409$, $m = 739$ for proliferating). Boxplot center line represents median, lower/upper box limits represent 25/75% quantiles, whiskers extend to box limit $\pm$ 1.5× interquartile range, and outlying points are plotted individually. **d–f**, Dynamic *HLA-DQA1* eQTL (rs3104371) in T cells ($n = 68$ individuals, $m = 82{,}423$ cells in synovium; $n = 909$, $m = 538{,}579$ in PBMC-blood). UMAP (**d**) colored by eQTL strength (β_{total}), from blue (weakest) to orange (strongest). Boxplots (**e**) showing the eQTL effects in cells from the top and bottom quintile of β_{total}, showing mean $\log_2(\text{UMI} + 1)$ per individual (*y* axis) by genotype. Labeled β_{NBME} and *P* value are derived from fitting the NBME model without cell-state interaction terms on the cells from the discrete quintile and comparing to a null model without genotype using an LRT. Boxplot elements defined as in **c**. Scatterplot (**f**) showing the mean β_{total} (*y* axis) compared to the mean $\log(\text{CP10k} + 1)$-normalized expression of *HLA-DQA1* (*x* axis) across annotated cell states (color). LRT, likelihood ratio test (one-sided).
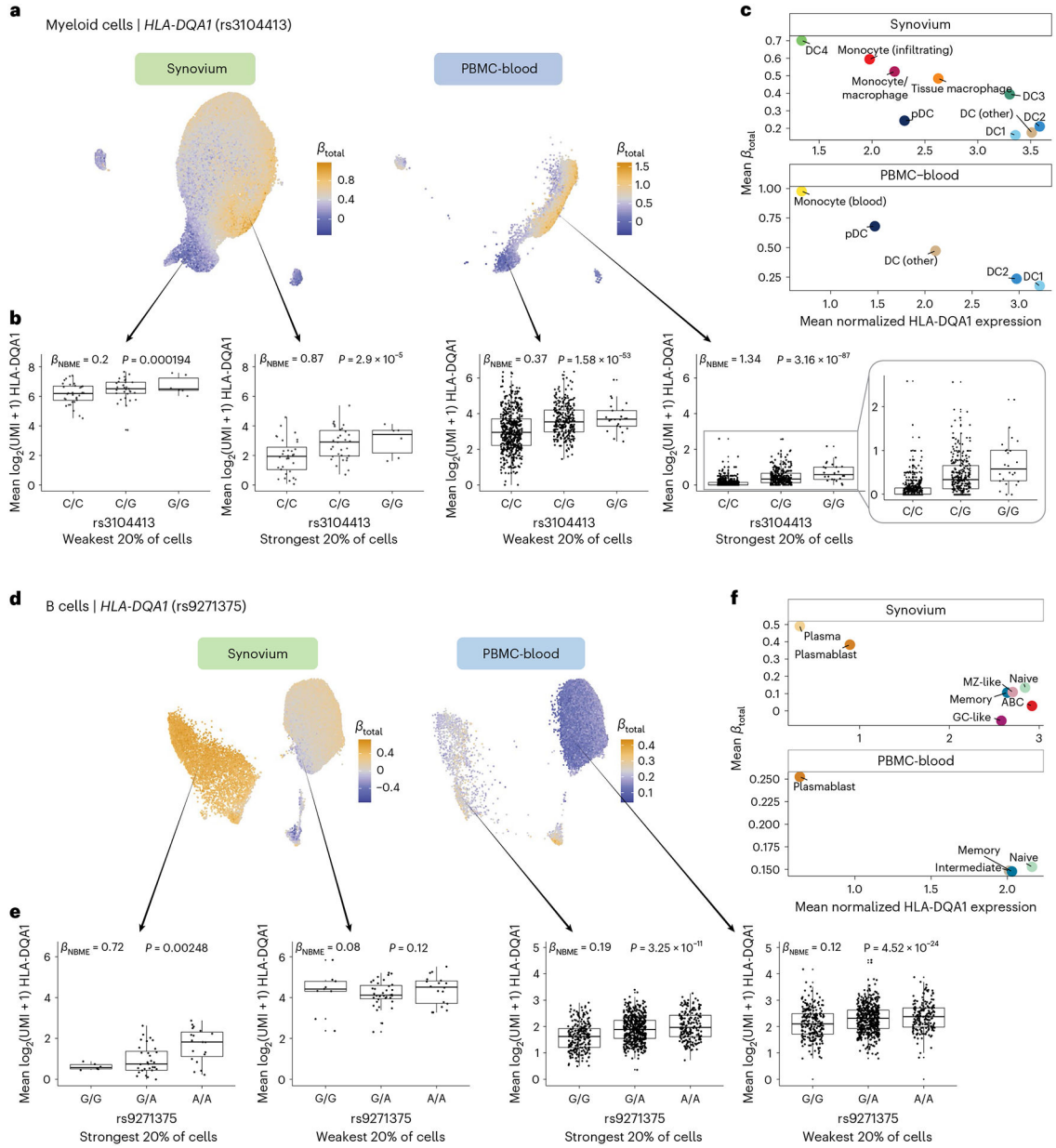
Fig. 6 |. Dynamic *HLA-DQ* eQTLs in myeloid and B cells.

a–c, Dynamic *HLA-DQA1* eQTL (rs3104413) in myeloid cells ($n = 69$ individuals, $m = 66,789$ cells in synovium; $n = 861$, $m = 40,568$ in PBMC-blood). UMAP (**a**) of cells for tissue-defined embedding, colored by β_{total}, from blue (weakest) to orange (strongest). Boxplot (**b**) showing the eQTL effect across individuals in the bottom and top quintiles of estimated β_{total}. Labeled β_{NBME} and *P* value are from fitting the NBME model without cell-state interaction terms on the cells from the discrete quintile and comparing to a null model without genotype using an LRT. Mean $\log_2(\text{UMI} + 1)$ across cells per individual (*y* axis) by each genotype. Boxplot center line represents median, lower/upper box limits represent 25/75% quantiles, whiskers extend to box limit $\pm$ 1.5× interquartile range, and outlying points are plotted individually. Scatterplot (**c**) showing the mean estimated β_{total} (*y* axis)

compared to the mean log(CP10k + 1)-normalized expression of *HLA-DQA1* (*x* axis) across annotated cell states (color). **d–f**, Dynamic *HLA-DQA1* eQTL in B cells (*n* = 65 individuals, *m* = 25,917 cells in synovium; *n* = 909 individuals, *m* = 80,784 in PBMC-blood). **d–f** are analogous to **a–c**, respectively. LRT, likelihood ratio test (one-sided).